

Emergence of Weyl metals driven by doped magnetic impurities in spin-orbit coupled semiconductors

Kyoung-Min Kim¹, Jinsu Kim², Soo-Whan Kim³, Myung-Hwa Jung², and Ki-Seok Kim¹

¹*Department of Physics, POSTECH, Pohang, Gyeongbuk 37673, Korea*

²*Department of Physics, Sogang University, Seoul 04107, Korea*

³*Max Planck POSTECH Center for Complex Phase Materials, Pohang, Gyeongbuk 37673, Korea*

(Dated: March 6, 2019)

The problem of dilute magnetic semiconductors leads our understanding on the interplay between correlations and disorders to be much deeper. In this study we propose a novel perspective, that is, a topological structure appears as a result of this interplay in a universal way. Constructing an effective field theory in terms of doped magnetic impurities (described by an $O(3)$ vector model with a random mass term), itinerant electrons of spin-orbit coupled semiconductors (given by a Dirac theory with a huge mass term), and effective interactions between doped magnetic ions and itinerant electrons (assumed by an effective Zeeman coupling term), we perform the perturbative renormalization group analysis in the one-loop level based on the dimensional regularization technique. As a result, we find that the mass renormalization in dynamics of itinerant electrons acquires negative feedback effects due to quantum fluctuations involved with the Zeeman coupling term, in contrast with that of the conventional problem of quantum electrodynamics, where such interaction effects enhance the fermion mass more rapidly. Recalling that the applied magnetic field decreases the band gap in the presence of spin-orbit coupling, this renormalization group analysis shows that the external magnetic field overcomes the renormalized band gap, allowed by doped magnetic impurities even without ferromagnetic ordering. In other words, the Weyl metal physics can be controlled by doping magnetic impurities into spin-orbit coupled semiconductors, even if the external magnetic field alone cannot realize the Weyl metal phase due to huge band gaps of semiconductors.

PACS numbers:

I. INTRODUCTION

The problem of doping magnetic impurities into semiconductors has been investigated for more than three decades, referred to as dilute magnetic semiconductors [1–3]. Here, several fundamental problems such as the nature of effective interactions between randomly doped magnetic impurities and the mechanism of spin polarization of itinerant electrons resulting from these random-positioned magnetic impurities had been discussed both extensively and intensively. Unfortunately, the final goal to achieve the ferromagnetic critical temperature of itinerant electrons above room temperature has not been reached, yet.

In the present study we propose completely a novel aspect in this long standing problem: A Weyl metal phase arises as a result of such doped magnetic impurities in spin-orbit coupled semiconductors under external magnetic fields. An essential point is that applied magnetic fields of the order of 10 T are much smaller than the band gap of original semiconductor samples without magnetic impurities, given by the order of $10^2\text{ meV} \sim 10^3\text{ meV}$. This implies that it is not possible to reach the Weyl metal phase only by applying external magnetic fields without doped magnetic impurities. Doping magnetic impurities such as Eu and Gd into spin-orbit coupled semiconductors, recent experiments could realize Weyl metal phases in $Eu_xBi_{2-x}Se_3$ and $Gd_xBi_{2-x}Te_{3-y}Se_y$, respectively, where the doping concentration covers from 2% to 4% approximately [4]. Here, transport measurements have shown that negative magneto-resistivity ap-

pears only when the applied magnetic field is in parallel with the applied electrical current [4], referred to as the negative longitudinal magneto-resistivity and regarded to be a fingerprint of the Weyl metallic state [5–7].

We investigate the role of doped magnetic impurities in spin-orbit coupled semiconductors, where gapped itinerant electrons are described by Dirac theory with a mass parameter. First, we consider the situation that magnetic impurities are randomly distributed in the vicinity of antiferromagnetic ordering [8]. This physical picture suggests an $O(3)$ vector model with the relativistic dispersion for the dynamics of randomly distributed magnetic impurities, where the distribution function of the random mass term is set to be Gaussian with a zero average value and a finite variance. Second, we assume that the dominant interaction channel between doped magnetic impurities and gapped itinerant electrons is described by the Zeeman term, reformulated as a chiral-current minimal coupling term, where the $O(3)$ vector field of the doped magnetic impurity plays the role of an emergent chiral gauge field in the dynamics of gapped itinerant electrons [9, 10].

Based on this effective field theory, we perform the perturbative renormalization group analysis up to the one-loop level. As a result, we find that the excitation gap for itinerant electrons of semiconductors acquires negative renormalization effects due to chiral current fluctuations driven by doped magnetic impurities. However, it turns out that the gap cannot be closed by such chiral-current fluctuations since their average vanishes in the vicinity of antiferromagnetic ordering. If ferromagnetic ordering

is considered, the chiral-current flowing phase is realized, nothing but the Weyl metal state [7, 9, 10]. Recent experiments have shown antiferromagnetic ordering at low temperatures for $Eu_xBi_{2-x}Se_3$ and $Gd_xBi_{2-x}Te_{3-y}Se_y$ [4]. Even if the gap cannot be closed by doped magnetic impurities alone, this situation opens new possibility: Applying external magnetic fields into these magnetically doped systems, renormalized band gaps would be closed to allow Weyl metal phases. Actually, our renormalization group analysis leads us to propose an interesting phase diagram in the plane of temperature and external magnetic field at a given disorder strength for magnetic impurities. A Weyl metal phase arises below a critical temperature and above a critical magnetic field, relatively low due to the role of doped magnetic impurities. In particular, we suggest a two-parameter scaling theory [7] for the longitudinal magnetoconductivity near the semiconductor to Weyl-metal transition.

The present manuscript is organized as follows. In Sec. II we construct an effective field theory for spin-orbit coupled semiconductors and doped magnetic impurities. In addition, we prepare for the renormalization group analysis, setting up the general structure of the renormalization group transformation. In Sec. III we perform the renormalization group analysis up to the one-loop level, based on the dimensional regularization. In Sec. IV we propose a phase diagram for our quantum phase transition from a spin-orbit coupled semiconducting phase to a Weyl metal phase, driven by doped magnetic impurities in the presence of external magnetic fields. In addition, we suggest a two-parameter scaling theory for the longitudinal magnetoconductivity near the semiconductor to Weyl-metal transition. In Sec. V we discuss some issues on recent experiments and conclude the present manuscript. In Appendixes we show all details of our perturbative renormalization group analysis, including the discussion on the stability of our renormalization group analysis beyond the one-loop level.

II. MODEL SYSTEM

A. Effective field theory

Our effective Hamiltonian consists of three main parts. The first describes the dynamics of electrons in topological or band insulators with strong spin-orbit coupling, given by a free Dirac theory as a minimal model,

$$\hat{H}_f = \sum_{\mathbf{k}} \psi_{\sigma\mathbf{a}\mathbf{k}}^\dagger (v\mathbf{k} \cdot \boldsymbol{\sigma}_{\sigma\sigma'} \otimes \tau_{ab}^z + mI_{\sigma\sigma'} \otimes \tau_{ab}^x) \psi_{\sigma'b\mathbf{k}}, \quad (1)$$

where the sign change of the mass parameter m gives rise to a topological phase transition from a topological insulating state to a normal band insulating phase [11]. Here, a (σ) is a band (spin) index. An important parameter is the excitation gap m of these electrons, given by the order of $10^2 \text{ meV} \sim 10^3 \text{ meV}$, which cannot be closed by external magnetic fields alone as discussed before.

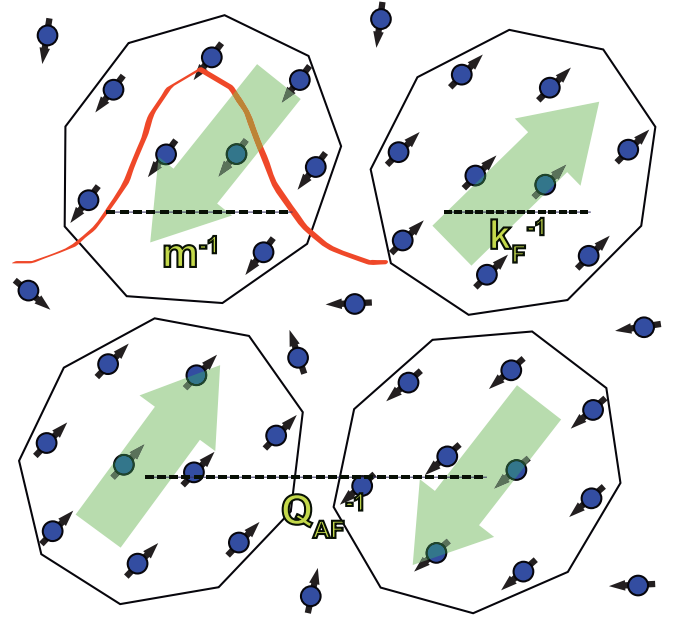


FIG. 1: A schematic physical picture of a spin-orbit coupled semiconductor doped with magnetic impurities. Black arrows with blue balls denote doped magnetic impurity spins. Black polygons represent ferromagnetic clusters, correlated with each other via effective antiferromagnetic interactions. Red curve expresses the electron's wave function envelope.

The second describes the dynamics of doped magnetic impurities. We propose an effective Hamiltonian for doped magnetic impurities as follows

$$\hat{H}_m = \sum_{ij} J_{ij} \mathbf{S}_i \cdot \mathbf{S}_j, \quad (2)$$

where J_{ij} is a random variable, described by a probability functional of $P[J_{ij}]$. An essential question is how these magnetic impurities interact with each other in this almost insulating host, i.e., the nature of J_{ij} and $P[J_{ij}]$ [1–3]. It turns out that samples in recent experiments are not in the insulating regime completely [4, 8]. Instead, resistivity measurements show quite a small number of metallic carriers. Although this aspect does not mean that the Ruderman-Kittel-Kasuya-Yosida (RKKY) interaction would be the mechanism of effective interactions between doped magnetic moments [12], where the dynamics of such electrons with a small Fermi surface would be essential to determine the nature of their effective interactions, we resort to this physical picture as our reference. The small Fermi surface leads us to consider ferromagnetic interactions dominantly between such magnetic moments, where the oscillating period of this effective interaction, given by the inverse of the Fermi momentum, is regarded to be quite long, compared with the average distance between magnetic impurities. As a result, it is natural to consider ferromagnetic clusters as coarse grained variables and their effective interactions. See Fig. 1. Measurements for spin susceptibility in recent experiments [4, 8] show that an antiferromagnetic

order appears around the order of 10 K , depending on physical properties of magnetic impurities in samples, of course, including the concentration. These experimental results drive us to construct an effective field theory for such ferromagnetic clusters Φ in the form of an O(3) vector model with a relativistic dispersion relation [8]

$$S_m = \int_0^\beta d\tau \int d^3\mathbf{r} \left\{ (\partial_\tau \Phi)^2 + c^2 (\partial_{\mathbf{r}} \Phi)^2 + (r + \delta r(\mathbf{r}))(\Phi \cdot \Phi) + \frac{u}{8}(\Phi \cdot \Phi)^2 \right\}. \quad (3)$$

Here, their random distributions in space are simulated by the introduction of a random mass term $\delta r(\mathbf{r})$, regarded to be the most relevant term in this formulation.

The most important third part is how these ferromagnetic clusters interact with electrons of the semiconductor host. Although it is not easy to determine the average size of such clusters, we propose an effective Zeeman interaction term between doped magnetic impurities and itinerant electrons, given by

$$\hat{H}_{int} = -\lambda \sum_i \psi_{i\sigma a}^\dagger \sigma_{\sigma\sigma'} \otimes \mathbf{I}_{ab} \psi_{i\sigma' b} \cdot \mathbf{S}_i. \quad (4)$$

This effective interaction term is quite special in the respect that the chiral matrix appears in the mathematical expression, where the ferromagnetic cluster field drives the chiral current along all directions of fluctuations [9, 10]. The mathematical formulation implies the conservation law of the U(1) chiral current. Indeed, the Ward identity is confirmed in the renormalization group analysis of the one-loop level, proven in Appendix B.

Based on the above discussion, we construct an effective free energy functional as follows

$$\begin{aligned} \mathcal{F} &= -\frac{1}{\beta} \int \mathcal{D}\delta r(\mathbf{r}) P[\delta r(\mathbf{r})] \ln \int \mathcal{D}\psi \mathcal{D}\Phi e^{-S_f - S_m - S_{int}}, \\ S_f &= \int_0^\beta d\tau \int d^3\mathbf{r} \bar{\psi} (\gamma_0 \partial_\tau - v\boldsymbol{\gamma} \cdot \partial_{\mathbf{r}} + m) \psi, \\ S_m &= \int_0^\beta d\tau \int d^3\mathbf{r} \left\{ (\partial_\tau \Phi)^2 + c^2 (\partial_{\mathbf{r}} \Phi)^2 + (r + \delta r(\mathbf{r}))(\Phi \cdot \Phi) + \frac{u}{8}(\Phi \cdot \Phi)^2 \right\}, \\ S_{int} &= -\int_0^\beta d\tau \int d^3\mathbf{r} \lambda \bar{\psi} \boldsymbol{\gamma} \psi \cdot \Phi. \end{aligned} \quad (5)$$

Here, the Dirac theory is reformulated in terms of Dirac gamma matrices, given by

$$\gamma_0 = \begin{pmatrix} 0 & 1 \\ 1 & 0 \end{pmatrix}, \quad \gamma_i = \begin{pmatrix} 0 & -\sigma_i \\ \sigma_i & 0 \end{pmatrix}, \quad \gamma_5 = \begin{pmatrix} 1 & 0 \\ 0 & -1 \end{pmatrix} \quad (6)$$

with $(i = 1, 2, 3)$, where $\psi = (\psi_{\uparrow 1} \ \psi_{\downarrow 1} \ \psi_{\uparrow 2} \ \psi_{\downarrow 2})^T$ is a Dirac spinor field. In particular, we point out that the Zeeman interaction term is rewritten in the form of the chiral-current and gauge-field minimal coupling term, where the three-component vector field of

Φ plays the role of the chiral gauge field. We assume the Gaussian distribution for the random mass, given by $P[\delta r(\mathbf{r})] = \mathcal{N} \int \mathcal{D}\delta r(\mathbf{r}) \exp[-\int \frac{d^3\mathbf{r} [\delta r(\mathbf{r})]^2}{2\Gamma_m}]$, where \mathcal{N} is the normalization constant and Γ_m is the variance.

Resorting to the replica trick for the disorder average [7, 9], we reformulate our effective field theory as follows

$$\begin{aligned} \mathcal{Z} &= \int \mathcal{D}(\bar{\psi}^{(a)}, \psi^{(a)}) \mathcal{D}\Phi^{(a)} e^{-S_f - S_m - S_{int}}, \\ S_f &= \int_0^\beta d\tau \int d^3\mathbf{r} \bar{\psi}^{(a)} (\gamma_0 \partial_\tau - v\boldsymbol{\gamma} \cdot \partial_{\mathbf{r}} + m) \psi^{(a)}, \\ S_m &= \int_0^\beta d\tau \int d^3\mathbf{r} \left\{ (\partial_\tau \Phi^{(a)})^2 + c^2 (\partial_{\mathbf{r}} \Phi^{(a)})^2 + r(\Phi^{(a)})^2 + \frac{u}{8}(\Phi^{(a)} \cdot \Phi^{(a)})^2 \right. \\ &\quad \left. - \int_0^\beta d\tau' \frac{\Gamma_m}{8} (\Phi_\tau^{(a)} \cdot \Phi_{\tau'}^{(a)}) (\Phi_{\tau'}^{(a')} \cdot \Phi_{\tau'}^{(a')}) \right\}, \\ S_{int} &= -\int_0^\beta d\tau \int d^3\mathbf{r} \lambda \bar{\psi}^{(a)} \boldsymbol{\gamma} \psi^{(a)} \cdot \Phi^{(a)}, \end{aligned} \quad (7)$$

where (a) is the replica index. We recall that fermions $(\psi^{(a)})$ represent semiconductor bands while bosons $(\Phi^{(a)})$ denote spin fluctuations of ferromagnetic clusters around antiferromagnetic ordering. They are characterized by the fermion velocity (v), the fermion mass (m), the boson velocity (c), and the boson mass (r). Bosons are self-interacting with their interaction strength (u), and disorder scattering with the disorder strength (Γ_m). Both fermions and bosons are interacting through the Zeeman coupling term with the interaction strength (λ). Total seven parameters define this effective field theory completely.

B. Setup for renormalization group analysis

1. Renormalized effective field theory within the dimensional regularization scheme

We take the double ε -expansion scheme [13], where all coupling constants of the self-interaction strength (u), the disorder strength (Γ_m), and the Zeeman interaction strength (λ) can be treated as perturbations. We generalize not only the space dimension ($3 \rightarrow d$) but also the time dimension ($1 \rightarrow d_\tau$). Then, the bare effective action is given by

$$\begin{aligned} S_f &= \int d^{d_\tau} \tau \int d^d \mathbf{r} \bar{\psi}^{(a)} (\boldsymbol{\gamma}_\tau \cdot \partial_\tau - v\boldsymbol{\gamma} \cdot \partial_{\mathbf{r}} + m) \psi^{(a)}, \\ S_m &= \int d^{d_\tau} \tau \int d^d \mathbf{r} \left\{ (\partial_\tau \Phi^{(a)})^2 + c^2 (\partial_{\mathbf{r}} \Phi^{(a)})^2 + r(\Phi^{(a)})^2 + \frac{u}{8}(\Phi^{(a)} \cdot \Phi^{(a)})^2 \right. \\ &\quad \left. - \int d^{d_\tau} \tau' \frac{\Gamma_m}{8} (\Phi_\tau^{(a)} \cdot \Phi_{\tau'}^{(a)}) (\Phi_{\tau'}^{(a')} \cdot \Phi_{\tau'}^{(a')}) \right\}, \\ S_{int} &= -\int d^{d_\tau} \tau \int d^d \mathbf{r} \lambda \bar{\psi}^{(a)} \boldsymbol{\gamma} \psi^{(a)} \cdot \Phi^{(a)}, \end{aligned} \quad (8)$$

where $\gamma_\tau = (\gamma_0, \dots, \gamma_{(d_\tau-1)})$ and $\gamma = (\gamma_1, \dots, \gamma_d)$ follow the Clifford algebra as $\{\gamma_{\tau i}, \gamma_j\} = 0$, $\{\gamma_{\tau i}, \gamma_{\tau j}\} = 2\delta_{ij}1_{2 \times 2}$, and $\{\gamma_i, \gamma_j\} = -2\delta_{ij}1_{2 \times 2}$.

Dimensional analysis gives scaling dimensions of $[\psi] = \frac{d+d_\tau-1}{2}$, $[\Phi] = \frac{d+d_\tau-2}{2}$, $[c] = 0$, $[m] = 1$, and

$$[u] = 4 - d - d_\tau, [\Gamma] = 4 - d, [\lambda] = \frac{4 - d - d_\tau}{2}. \quad (9)$$

This leads us to set $d_\tau = \varepsilon_\tau$ and $d = 4 - \varepsilon - \varepsilon_\tau$ in the loop calculation so that all coupling constants are put into the perturbative regime, where $[u] = \varepsilon$, $[\Gamma] = \varepsilon + \varepsilon_\tau$, and $[\lambda] = \frac{\varepsilon}{2}$. In principle, we set $\varepsilon_\tau = 1$ and $\varepsilon = 0$ in the last stage. Here, the fermion velocity v is set to be unity. As a result, we have total six parameters to characterize our effective field theory.

Introducing all counterterms to cancel UV divergences from quantum fluctuations into the above bare action, we have an effective renormalized action

$$\begin{aligned} S_f &= \int d^{d_\tau} \tau \int d^d \mathbf{r} \bar{\psi}_r^{(a)} (Z_0 \gamma_\tau \cdot \partial_\tau - Z_1 \gamma \cdot \partial_r \\ &\quad + \mu Z_m m_r) \psi_r^{(a)}, \\ S_m &= \int d^{d_\tau} \tau \int d^d \mathbf{r} \left\{ Z_2 (\partial_\tau \Phi_r^{(a)})^2 + Z_c c_r^2 (\partial_r \Phi_r^{(a)})^2 \right. \\ &\quad + \mu^2 Z_r r_r (\Phi_r^{(a)})^2 + \frac{\mu^\varepsilon Z_u u_r}{8} (\Phi_r^{(a)} \cdot \Phi_r^{(a)})^2 \\ &\quad \left. - \int_{\tau'} \frac{\mu^{\varepsilon+\varepsilon_\tau} Z_{\Gamma_m} \Gamma_{mr}}{8} (\Phi_{\tau r}^{(a)} \cdot \Phi_{\tau' r}^{(a)}) (\Phi_{\tau' r}^{(a')} \cdot \Phi_{\tau r}^{(a')}) \right\}, \\ S_{int} &= - \int d^{d_\tau} \tau \int d^d \mathbf{r} Z_\lambda \mu^{\varepsilon/2} \lambda_r \bar{\psi}_r^{(a)} \gamma \gamma_5 \psi_r^{(a)} \cdot \Phi_r^{(a)}. \quad (10) \end{aligned}$$

Here, μ is a renormalization scale ($[\mu] = 1$). Field renormalization factors are introduced to relate bare fields with renormalized ones as follows: $\psi = Z_\psi^{1/2} \bar{\psi}_r$ and $\Phi = Z_\Phi^{1/2} \Phi_r$ with $Z_\psi = Z_1 (Z_0/Z_1)^{d_\tau}$ and $Z_\Phi = Z_2 (Z_0/Z_1)^{d_\tau-2}$, where the subscript r means “renormalized”. All other renormalized parameters are given by

$$\begin{aligned} m_r &= \mu^{-1} (Z_1/Z_m) m, \\ c_r &= (Z_2/Z_c)^{1/2} (Z_0/Z_1)^{-1} c, \\ r_r &= \mu^{-2} (Z_2/Z_r) (Z_0/Z_1)^{-2} r, \\ \lambda_r &= \mu^{-\frac{\varepsilon}{2}} Z_2^{1/2} (Z_0/Z_1)^{-1+\varepsilon_\tau/2} \lambda, \\ u_r &= \mu^{-\varepsilon} (Z_2^2/Z_u) (Z_0/Z_1)^{-4+\varepsilon_\tau} u, \\ \Gamma_{mr} &= \mu^{-\varepsilon-\varepsilon_\tau} (Z_2^2/Z_{\Gamma_m}) (Z_0/Z_1)^{-4} \Gamma_m, \quad (11) \end{aligned}$$

where the Ward identity of $Z_1 = Z_\lambda$ has been used.

Counterterms are given by singular quantum corrections

$$\begin{aligned} \delta_0 \gamma_0 &= -i \partial_{k_0} \Sigma(k), \quad \delta_1 \gamma = \partial_k \Sigma(k), \quad \delta_m m = \Sigma(k)|_{k=0}, \\ \delta_2 &= \partial_{q_0^2} \Pi(q), \quad \delta_c = \partial_{q^2} \Pi(q), \quad \delta_r r = \Pi(q)|_{q=0}, \\ \delta_\lambda &= -\lambda^{-1} \sum_i \delta \lambda(i), \quad \delta_u = u^{-1} \sum_i \delta u(i), \\ \delta_{\Gamma_m} &= -\Gamma_m^{-1} \sum_i \delta \Gamma_m(i), \quad (12) \end{aligned}$$

where all renormalization factors are related to these counterterms as $Z_0 = 1 + \delta_0$, $Z_1 = 1 + \delta_1$, $Z_m = 1 + \delta_m$, $Z_2 = 1 + \delta_2$, $Z_c = 1 + \delta_c$, $Z_r = 1 + \delta_r$, $Z_u = 1 + \delta_u$, $Z_{\Gamma_m} = 1 + \delta_{\Gamma_m}$, and $Z_\lambda = 1 + \delta_\lambda$. Here, we resort to the minimal subtraction scheme and use the convention of $G^{-1}(k) = G_0^{-1}(k) - \Sigma(k)$ and $D^{-1}(k) = D_0^{-1}(q) - \Pi(q)$. $\Sigma(k)$ ($\Pi(q)$) are singular self-energy corrections for fermions (bosons), $\delta \lambda(i)$ are singular fermion-boson vertex corrections, $\delta u(i)$ are singular boson self-interaction vertex corrections, and $\delta \Gamma_m(i)$ are singular boson disorder-scattering vertex corrections. The meaning of i will be clarified below, used to identify various Feynman diagrams.

2. Renormalization group equations

The renormalized Green's function is defined as

$$\begin{aligned} &\langle \bar{\psi}_r(k_1) \cdots \psi_r(k_{m+1}) \cdots \Phi_r(k_{2m+1}) \cdots \rangle \\ &= G^{(m,n)}(\{k_i\}; \mathbf{F}, \mu) \delta^{d+d_\tau} \left(\sum_{i=1}^m k_i - \sum_{j=m+1}^{2m+n} k_j \right), \quad (13) \end{aligned}$$

where the coupling constants are put into a vector form of $\mathbf{F} = (\lambda, u, \Gamma_m, m, c, r)$. This is related to the bare Green's function as

$$\begin{aligned} &G^{(m,n)}(\{k_i\}; \mathbf{F}, \mu) \\ &= Z_\psi^{-m} Z_\Phi^{-\frac{n}{2}} (Z_0/Z_1)^{-\varepsilon_\tau} G_B^{(m,n)}(\{k_{Bi}\}; \mathbf{F}_B). \quad (14) \end{aligned}$$

It is straightforward to show that the renormalized Green's function satisfies the following differential equation, referred to as the Callan-Symanzik equation for the Green's function,

$$\begin{aligned} &\left\{ \sum_{i=1}^{2m+n} \left(z \mathbf{k}_{\tau,i} \cdot \nabla_{\mathbf{k}_{\tau,i}} + \mathbf{k}_i \cdot \nabla_{\mathbf{k}_i} \right) - \beta \cdot \nabla_{\mathbf{F}} \right. \\ &\quad - 2m \left(-\frac{5-\varepsilon}{2} + \eta_\psi \right) - n \left(-\frac{6-\varepsilon}{2} + \eta_\phi \right) \\ &\quad \left. - \varepsilon_\tau (z-1) - (4-\varepsilon) \right\} G^{(m,n)}(\{k_i\}; \mathbf{F}, \mu) = 0. \quad (15) \end{aligned}$$

Here, beta functions are expressed in terms of renormalization factors as follows

$$\begin{aligned} \beta_\lambda &= \lambda \left[-\frac{\varepsilon}{2} - \left(1 - \frac{\varepsilon_\tau}{2} \right) (z-1) + \frac{1}{2} \frac{\partial \ln Z_2}{\partial \ln \mu} \right], \\ \beta_u &= u \left[-\varepsilon - (4-\varepsilon_\tau)(z-1) + \frac{\partial \ln (Z_2^2/Z_u)}{\partial \ln \mu} \right], \\ \beta_{\Gamma_m} &= \Gamma_m \left[-\varepsilon - \varepsilon_\tau - 4(z-1) + \frac{\partial \ln (Z_2^2/Z_{\Gamma_m})}{\partial \ln \mu} \right], \\ \beta_c &= c \left[-(z-1) + \frac{1}{2} \frac{\partial \ln (Z_2/Z_c)}{\partial \ln \mu} \right], \\ \beta_m &= m \left[-1 + \frac{\partial \ln (Z_1/Z_m)}{\partial \ln \mu} \right], \\ \beta_r &= r \left[-2 - 2(z-1) + \frac{\partial \ln (Z_2/Z_r)}{\partial \ln \mu} \right], \quad (16) \end{aligned}$$

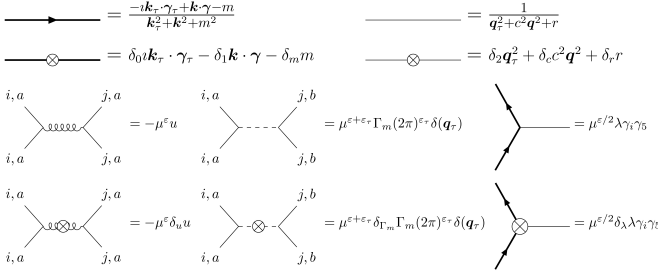


FIG. 2: Feynman rules in momentum space. The first line represents fermion and boson propagators, respectively. The second line expresses counterterms for fermion and boson propagators, respectively. The third line describes three types of vertices for boson self-interactions, boson disorder scattering, and fermion-boson Zeeman interactions, respectively. The last line denotes counterterms for all interaction vertices described by the third line.

where we defined $\beta_\lambda \equiv \frac{\partial \lambda}{\partial \ln \mu}$, $\beta_u \equiv \frac{\partial u}{\partial \ln \mu}$, $\beta_{\Gamma_m} \equiv \frac{\partial \Gamma_m}{\partial \ln \mu}$, $\beta_c \equiv \frac{\partial c}{\partial \ln \mu}$, and $\beta_r \equiv \frac{\partial r}{\partial \ln \mu}$. z is the dynamical critical exponent, introduced to incorporate the space-time anisotropy. η_ψ (η_Φ) is the anomalous scaling dimension for the fermion (boson) field, describing its fractal behavior. They are given by

$$z = 1 + \frac{\partial \ln(Z_0/Z_1)}{\partial \ln \mu}, \quad \eta_\psi = \frac{1}{2} \frac{\partial \ln Z_1}{\partial \ln \mu} + \frac{\varepsilon_\tau}{2}(z-1),$$

$$\eta_\Phi = \frac{1}{2} \frac{\partial \ln Z_2}{\partial \ln \mu} + \left(\frac{\varepsilon_\tau}{2} - 1 \right)(z-1). \quad (17)$$

Solving the Callan-Symanzik equation at the fixed point, given by the fact that all beta functions vanish, we obtain the scaling expressions for both Green's functions of fermions and bosons, respectively,

$$G(\mathbf{k}_\tau, \mathbf{k}) = \frac{1}{|\mathbf{k}|^{1-\varepsilon_\tau(z-1)-2\eta_\psi}} \tilde{g}(|\mathbf{k}_\tau|^{1/z}/|\mathbf{k}|),$$

$$D(\mathbf{q}_\tau, \mathbf{q}) = \frac{1}{|\mathbf{q}|^{2-\varepsilon_\tau(z-1)-2\eta_\Phi}} \tilde{d}(|\mathbf{q}_\tau|^{1/z}/|\mathbf{q}|). \quad (18)$$

Here, $\tilde{g}(|\mathbf{k}_\tau|^{1/z}/|\mathbf{k}|)$ ($\tilde{d}(|\mathbf{q}_\tau|^{1/z}/|\mathbf{q}|)$) is the scaling function of the fermion (boson) propagator, which should be found by explicit calculations, not trivial.

III. RENORMALIZATION GROUP ANALYSIS

A. Self-energy corrections

Based on the renormalized effective action, we introduce Feynman rules as shown in Fig. 2. Here, the thick line represents an electron propagator, and the thin line describes the Green's function of an order-parameter field. The spring line means an effective self-interaction between order parameter fluctuations, and the dotted line gives an interaction vertex involved with disorder.

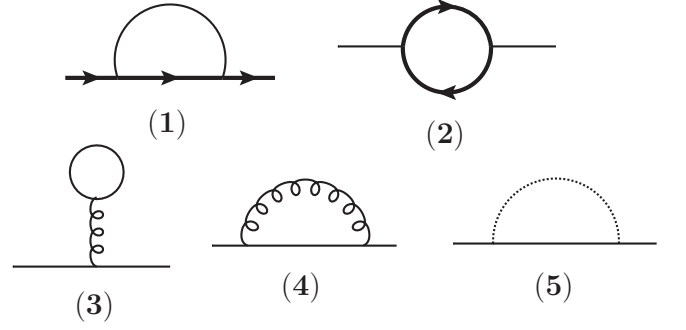


FIG. 3: Self-energy corrections for both fermions and bosons. The first diagram is the fermion's self-energy and the others are the boson's self-energy corrections.

The \otimes -symbol describes a counterterm for each propagator and each vertex. Resorting to these Feynman rules, one can take into account quantum fluctuations perturbatively, where the dimensional regularization scheme is utilized.

The fermion self-energy is shown in Fig. 3-(1). The calculation is similar to that of quantum electrodynamics (QED) [14]. Here, we summarize our results

$$Z_0 - 1 = -\frac{3\lambda^2}{4\pi^2 \varepsilon c(1+c)^2},$$

$$Z_1 - 1 = -\frac{(1+2c)\lambda^2}{12\pi^2 \varepsilon c(1+c)^2},$$

$$Z_m - 1 = +\frac{3\lambda^2}{4\pi^2 \varepsilon c(1+c)}, \quad (19)$$

where all integral details are shown in Appendix A 1. The main difference compared to QED is the fact that the anomalous dimension of the fermion mass is positive, i.e., $Z_m - 1 > 0$. In other words, the electron mass is *reduced* by spin fluctuations while it is enhanced by gauge fluctuations in QED. This is an unusual feature given by chiral gauge-field fluctuations. There exist other differences. The boson velocity appears in the renormalization factors because of the absence of the Lorentz symmetry ($c \neq v = 1$). The numerator factors also differ from those of QED because there is no time-component here for chiral gauge-field fluctuations, i.e., $\Phi_0 = 0$.

The other diagrams in Fig. 3 are for boson self-energy corrections. The calculation of Fig. 3-(2) is similar to that of QED while integrals of the others are in parallel with those of the ϕ^4 -theory. We also summarize our results only

$$Z_2 - 1 = -\frac{\lambda^2}{6\pi^2 \varepsilon} - \frac{4\Gamma_m}{(4\pi)^{3/2}(\varepsilon + \varepsilon_\tau)c^3},$$

$$Z_c - 1 = -\frac{\lambda^2}{6\pi^2 \varepsilon c^2},$$

$$Z_r - 1 = \frac{5u}{16\pi^2 \varepsilon c^3} - \frac{4\Gamma_m}{(4\pi)^{3/2}(\varepsilon + \varepsilon_\tau)c^3}, \quad (20)$$

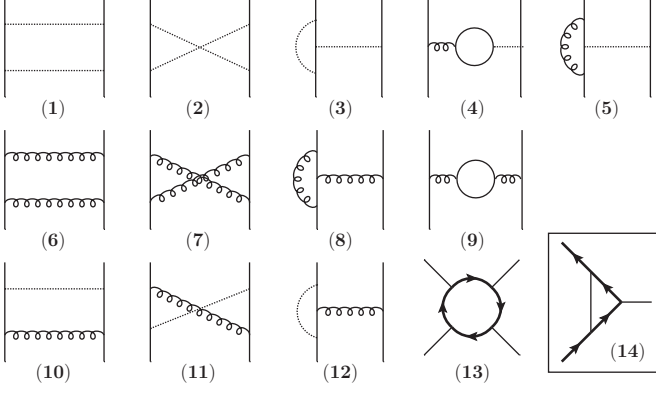


FIG. 4: Three types of vertex corrections. Vertex corrections for the disorder scattering are in the first line, and those for the boson interaction, in the second and the third line. The last diagram in the third line should be interpreted as an amputated diagram. The diagram in the box is the correction in the one-loop order for the Zeeman coupling.

where all details involved with integrals are shown in Appendix A 2. The Zeeman coupling term results in negative field renormalization, which may be interpreted as screening effects for all coupling constants. The disorder scattering causes additional field renormalization, identified with additional screening effects. This additional field renormalization also decreases the boson velocity while the boson mass is unaffected by the disorder scattering since the effect on it is canceled by the Γ_m term in Z_r . The boson self-interaction increases the boson mass as well known in the ϕ^4 -theory while it doesn't give the field renormalization in the one loop order [14].

B. Vertex corrections

Vertex corrections are shown in Fig. 4. The calculation is standard, similar to the ϕ^4 -theory for diagrams from Fig. 4(1) to Fig. 4(12) and QED for Fig. 4(13) and Fig. 4(14), though one should be careful about the mixing of the boson interaction and the disorder scattering, shown in Fig. 4(4), Fig. 4(5), Fig. 4(10), Fig. 4(11), and Fig. 4(12). Our results are summarized as

$$\begin{aligned} Z_\lambda - 1 &= -\frac{\lambda^2(1+2c)}{12\pi^2c(1+c)^2\varepsilon}, \\ Z_u - 1 &= \frac{11u}{16\pi^2c^3\varepsilon} - \frac{12\Gamma_m}{(4\pi)^{3/2}c^3(\varepsilon + \varepsilon_\tau)}, \\ Z_{\Gamma_m} - 1 &= -\frac{8\Gamma_m + 12u}{(4\pi)^{3/2}c^3(\varepsilon + \varepsilon_\tau)} + \frac{u}{4\pi^2c^3\varepsilon}. \end{aligned} \quad (21)$$

See Appendix A 3 for more details. We point out that $Z_\lambda = Z_1$ is satisfied by the Ward identity (Appendix B). The diagram Fig. 4(13) possibly gives renormalization for the boson interaction. However, it turns out to vanish by the Ward identity. The disorder scattering gives an

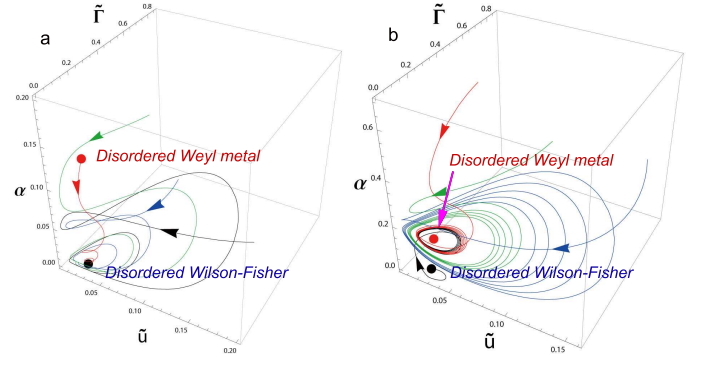


FIG. 5: Two types of fixed points described by the beta functions in Eq. (22). We introduce dimensionless couplings as $\alpha \equiv \frac{\lambda^2}{12\pi^2}$, $\tilde{u} \equiv \frac{u}{16\pi^2c^3}$, and $\tilde{\Gamma} \equiv \frac{2\Gamma_m}{(4\pi)^{3/2}c^3}$. (a) When $\varepsilon = 0.01$, the boson interaction strength and the disorder strength are finite while the boson velocity and the Zeeman interaction strength vanish in the low-energy limit. This corresponds to the disordered Wilson-Fisher fixed point. (b) When $\varepsilon = 0.3$, all coupling constants are finite. This fixed point is identified as a disordered Weyl metal phase in that the fermion mass parameter gets the negative feedback from the Zeeman interaction term, and the Weyl metallic phase may arise in the presence of external magnetic fields.

antiscreening effect while the boson interaction causes a screening effect in the renormalization of the boson interaction and the disorder scattering.

C. Beta functions and fixed points

Inserting all renormalization factors of Eqs. (19), (20), and (21) into the formal expressions for the beta functions Eq. (16), we obtain

$$\begin{aligned} \beta_\lambda &= \lambda \left[-\frac{\varepsilon}{2} + \frac{(c^3 + 2c^2 + 2c - 4)\lambda^2}{12\pi^2c(1+c)^2} + \frac{2\Gamma_m}{(4\pi)^{3/2}c^3} \right], \\ \beta_u &= u \left[-\varepsilon + \frac{(4c^3 + 8c^2 + 10c - 24)\lambda^2}{12\pi^2c(1+c)^2} \right. \\ &\quad \left. + \frac{11u}{16\pi^2c^3} - \frac{4\Gamma_m}{(4\pi)^{3/2}c^3} \right], \\ \beta_{\Gamma_m} &= \Gamma_m \left[-1 - \varepsilon + \frac{(4c^3 + 8c^2 + 12c - 32)\lambda^2}{12\pi^2c(1+c)^2} \right. \\ &\quad \left. + \frac{(24\sqrt{\pi} + 4)u}{16\pi^2c^3} \right], \\ \beta_m &= m \left[-1 + \frac{(10 + 11c)\lambda^2}{12\pi^2c(1+c)^2} \right], \\ \beta_c &= c \left[\frac{(c^4 + 2c^3 + 2c^2 - 10c - 1)\lambda^2}{12\pi^2c^2(1+c)^2} + \frac{2\Gamma_m}{(4\pi)^{3/2}c^3} \right], \\ \beta_r &= r \left[-2 + \frac{(c^3 + 2c^2 + 3c - 8)\lambda^2}{6\pi^2c(1+c)^2} + \frac{5u}{16\pi^2c^3} \right], \end{aligned} \quad (22)$$

which describe the evolution of all coupling parameters as a function of an energy scale, where $\varepsilon_\tau = 1$.

The limit of $\lambda \rightarrow 0$ reproduces the β -functions of the $O(3)$ vector model with a random mass term as expected [14]. On the other hand, the existence of the λ vertex involved with effective interactions between magnetic clusters and itinerant electrons gives rise to serious modifications on the fixed-point structure. One may point out that the λ vertex is essentially the same as that of QED, regarded to be a $U(1)$ gauge coupling constant. Indeed, we confirm the Ward identity, given by Appendix B in spite of the presence of the chiral matrix. However, there exists an essential different aspect between our chiral-gauge vertex and the $U(1)$ gauge vertex of QED. The sign of the mass renormalization given by the one-loop quantum correction shows negativity instead of positivity. We recall the mass renormalization in QED, given by Ref. [14]. This “negative” quantum correction in the chiral-gauge interaction vertex opens the possibility for the emergence of a Weyl metal phase, driven by doped magnetic impurities.

In order to verify this possibility, we solve these renormalization group equations and find two types of fixed points. They are allowed to exist until $\varepsilon < 0.3103$, which we cannot find any fixed points beyond. In the region of $0 \leq \varepsilon < 0.0832$, the Zeeman coupling constant vanishes while both the self-interaction and disorder parameters remain finite, which is nothing but the disorder fixed point of the $O(3)$ vector model with a random mass term. In the region of $0.0832 < \varepsilon < 0.3103$, all coupling constants are finite, identified with an interacting fixed point between itinerant electrons and doped magnetic impurities. See Fig. 5. The reason why this interacting fixed point is allowed only within this ε region is that for non-vanishing λ_* , ε should be large enough to overcome the screening of the disorder scattering in β_λ , i.e., $\frac{\varepsilon}{2} > \frac{2(\Gamma_m/c^3)_*}{(4\pi)^{3/2}}$ while the upper limit of 0.3103 comes from the stability condition of the fixed point. This means that only in quasi-two dimensional systems, the Zeeman coupling can play a central role in low energy physical phenomena.

This nontrivial fixed point is given by

$$\begin{aligned} \lambda_* &= 6.90 + 2.45 \ln \varepsilon, \quad u_* = 4.05 + 0.773\varepsilon, \\ \Gamma_{m*} &= 1.03 + 2.45\varepsilon, \quad c_* = 1.37 - 0.0216\varepsilon^{-1.5}, \end{aligned} \quad (23)$$

where the critical exponents near this fixed point are

$$\begin{aligned} z &= 1.01 + 0.394\varepsilon, \quad \eta_\psi = -0.0427 + 3.46\varepsilon, \quad \eta_\Phi = 5\varepsilon, \\ \nu_m^{-1} &= 1.08 - 1.99\varepsilon, \quad \nu_r^{-1} = 1.97 - 0.411\varepsilon. \end{aligned} \quad (24)$$

The scaling laws of both fermions and bosons are corrected. Especially, the scaling of the fermion mass (ν_m^{-1}) is fairly nontrivial. It decreases proportionally to ε due to the screening effect of the Zeeman coupling. For example, $\nu_m^{-1} = 1$ in the free theory becomes $\nu_m^{-1} = 0.46$ at $\varepsilon = 0.31$. As a result, the increasing rate of the fermion mass becomes smaller. This allows an external magnetic field to overcome the mass gap.

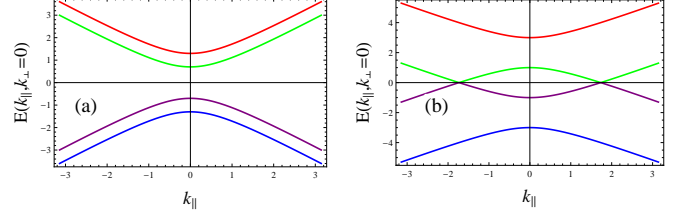


FIG. 6: Band structures of spin-orbit coupled semiconductors with Zeeman splitting. (a) Bands are gapped when the magnetic field is smaller than the band gap while (b) a pair of Weyl points appear at the Fermi level when the magnetic field is larger than the band gap.

IV. EMERGENCE OF WEYL METALS FROM MAGNETICALLY DOPED SPIN-ORBIT COUPLED SEMICONDUCTORS

A. Applying external magnetic fields

We introduce an external magnetic field coupled to the fermions in the following way [9]

$$S_h = \int d^d\tau \tau \int d^d\mathbf{r} \bar{\psi} \mathbf{h} \cdot \gamma \gamma_5 \psi. \quad (25)$$

This magnetic field makes two bands of two-fold degeneracy split into four bands as (Fig. 6)

$$E(\mathbf{k}) = \pm \sqrt{\mathbf{k}_{\perp}^2 + \left(|\mathbf{h}| \pm \sqrt{m^2 + \mathbf{k}_{\parallel}^2} \right)^2}, \quad (26)$$

where $\mathbf{k}_{\parallel} = \mathbf{h}(\mathbf{k} \cdot \mathbf{h})/|\mathbf{h}|^2$ and $\mathbf{k}_{\perp} = \mathbf{k} - \mathbf{k}_{\parallel}$. When $|\mathbf{h}| = h > m$, the mass gap is closed and a Weyl semimetal appears.

An idea is that although the mass gap is too large to overcome by external magnetic fields, taking into account renormalization effects by doped magnetic impurities allows the gap closing as a function of the applied magnetic field and the temperature. The renormalized action of Eq. (25) is

$$S_h = \int d^d\tau \tau \int d^d\mathbf{r} Z_h \bar{\psi}_r \mathbf{h}_r \cdot \gamma \gamma_5 \psi_r, \quad (27)$$

where the renormalized magnetic field is related with the bare magnetic field as $\mathbf{h}_r = \mu^{-1}(Z_1/Z_h)\mathbf{h}$. Then, the beta function for h_r is given by

$$\beta_h = h \left[-1 + \frac{\partial \ln(Z_h/Z_1)}{\partial \ln b} \right] = -h. \quad (28)$$

We note that there is no quantum correction for h_r in the one-loop level, consistent with the Ward identity.

Solving renormalization group equations of $\beta_h = -h(\mu)$, $\beta_m = -(1/\nu_m)m(\mu)$, $\beta_T = -zT(\mu)$, we find

$$h(\mu) = h\mu^{-1}, \quad m(\mu) = m\mu^{-1/\nu_m}, \quad T(\mu) = T\mu^{-z}, \quad (29)$$

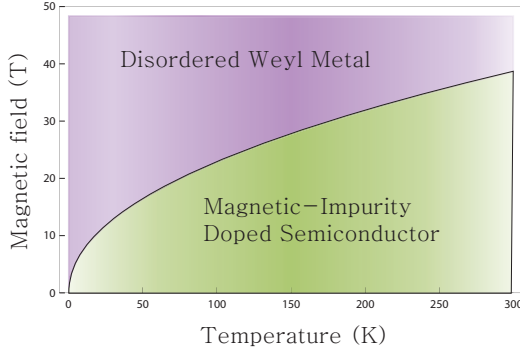


FIG. 7: Phase diagram based on Eq. (31). Here, we utilized $z = 1.13$, $\nu_m = 2.15$, $T_0 = 300$ [K], $m = 0.3$ [eV], and $g_s = 100$ for parameters.

which shows how these parameters are renormalized by the presence of doped magnetic impurities as a function of an energy scale μ .

A Weyl semimetal appears when $h(\mu) > m(\mu)$, which means $h/m > \mu^{1-1/\nu_m}$. Replacing the scaling parameter with temperature and fixing the scale of $T(\mu) = T_0$, we find the gap closing condition

$$\left(\frac{h}{m}\right)_c = \left(\frac{T}{T_0}\right)^{\frac{\nu_m-1}{z\nu_m}}. \quad (30)$$

Physical units are brought back as $h = g_s \mu_B H$, where g_s , μ_B , and H are the Lande g-factor of the electron's spin, the Bohr magneton, and the external magnetic field, respectively. As a result, we obtain the critical field strength given by

$$H_c = (m/g_s \mu_B) \left(\frac{T}{T_0}\right)^{0.474}, \quad (31)$$

which gives rise to the phase diagram of Fig. 7. For a numerical estimate, we used $z = 1.13$ and $\nu_m = 2.15$ at $\varepsilon = 0.310$, where the anomalous scaling dimensions are maximized.

Figure 7 shows a phase diagram based on Eq. (31). The external magnetic field can turn spin-orbit coupled semiconductors into Weyl semimetals by closing the band gap. The critical strength of the field is huge in the high temperature regime, for example, $H_c(T = 300 \text{ [K]}) = 52$ [T]. However, $H_c(T)$ becomes much smaller at low temperatures because the mass gap gets screened by spin fluctuations while the magnetic field is unaffected. Using $T_0 = 300$ [K] as an UV energy scale and $m = 0.3$ [eV], $g_s = 100$ for typical values at that scale, we find $H_c = 3.46 * T^{0.474}$. At temperature $T = 10$ [K], we have

$$H_c = 8.01 \text{ [T]} \text{ (at } T = 10 \text{ [K])}. \quad (32)$$

B. Negative longitudinal magneto-resistivity

The existence of a topological phase transition from either a topological or band insulating state to a Weyl

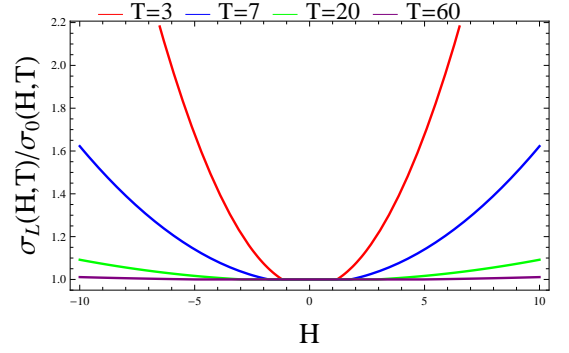


FIG. 8: Longitudinal magnetoconductivities in Weyl semimetals. The conductivities are normalized with the Drude conductivity. For parameters, $a = 0.2$ and $b = 0.1$ are used.

metal phase has been confirmed by our renormalization group analysis. Although this demonstration itself touches a novel aspect in the study of dilute magnetic semiconductors, it is necessary to verify the present scenario more quantitatively. Here, we focus on the longitudinal magneto-resistivity, which acquires an essential modification in the Weyl metal state, given by

$$\sigma_L(H, T) = \sigma_0(T)(1 + C_W H^2), \quad (33)$$

where $\sigma_0(T)$ is the Drude conductivity with a weak anti-localization quantum correction and C_W is a positive coefficient with the applied magnetic field along the direction of the electric field [5]. This modification has been proposed to originate from the chiral anomaly [15–18], where $C_W H^2 \sim h^2 - m^2$ corresponds to the square of the momentum-space distance between a pair of Weyl points [5, 9, 10] given by $k_{\parallel} = \sqrt{h^2 - m^2}$ from Eq. (26).

Introducing renormalization effects from renormalization group equations into this expression, given by Eq. (29), we find

$$C_W(H, T) = \frac{a}{T^{2/z}} - \frac{b}{H^2 T^{2/z\nu_m}}, \quad (34)$$

where $a \propto g_s^2$ and $b \propto m^2$ are regarded to be phenomenological fitting parameters [4]. Note that C_W depends not only temperature but also external magnetic fields. This is not the case in usual Weyl semimetals, where C_W is just a coefficient of the negative MR [7]. This is a characteristic feature of Weyl semimetals arising from magnetically doped spin-orbit coupled semiconductors [4].

Figure 8 shows longitudinal conductivities normalized with the Drude conductivity, given by

$$\sigma_L(H, T)/\sigma_0(H, T) = 1 + \left(\frac{a}{T^{1.78}} - \frac{b}{H^2 T^{0.838}} \right) H^2, \quad (35)$$

where we used $z = 1.13$ and $\nu_m = 2.15$ for a numerical estimate. Positive magneto-conductivities start at $H_c = 1.2, 1.8, 2.9, 4.9$ for $T = 3, 7, 20, 60$, respectively. Moreover, the positive magneto-conductivity is significantly enhanced as temperature is lowered.

V. SUMMARY AND DISCUSSION

Constructing an effective field theory for magnetically doped spin-orbit coupled semiconductors [Eq. (5)], we performed the renormalization group analysis [Eqs. (15), (16), and (17)] and obtained beta functions [Eq. (22)] for all coupling parameters (the fermion-boson Zeeman interaction, the boson self-interaction, the disorder scattering, the fermion mass, the boson velocity, and the boson mass), evaluating Feynman diagrams up to the one-loop level [Eqs. (19), (20), and (21)]. Solving these renormalization group equations, we found an interacting fixed point [Eq. (23)] and revealed how all parameters evolve as a function of temperature near the fixed point [Eq. (24)]. In particular, we proposed a phase diagram in the plane of the applied magnetic field and temperature at a given concentration of magnetic impurities based on Eq. (31) [Fig. 7]. In addition, we suggested the temperature & magnetic-field evolution for the longitudinal magnetoconductivity [Eqs. (34) and (35)] at low temperatures, where the Weyl metal phase is realized, given by Fig. 8.

Recently, we applied the present scenario to magnetically doped spin-orbit coupled semiconductors such as $Eu_xBi_{2-x}Se_3$ and $Gd_xBi_{2-x}Te_{3-y}Se_y$ [4]. Actually, we could fit the temperature evolution for the enhancement factor C_W of the longitudinal magnetoconductivity at low temperatures, where a Weyl metallic state is realized. Furthermore, experiments could extract out a phase diagram in the plane of the applied magnetic field and temperature at a given concentration of magnetic impurities, taking into account the maximum point of the longitudi-

nal magnetoresistivity, which determines a critical magnetic field at a given temperature. It turns out that such a phase diagram is consistent with our proposed phase diagram.

One unsatisfactory point in our renormalization group analysis is that the regularization parameter ε was utilized as a phenomenological fitting parameter. Theoretically speaking, it should be chosen as $\varepsilon \rightarrow 0$ in the last stage. However, the interacting fixed point turns out not to exist in the exactly three dimensional space. If we accept $\varepsilon = 0.31$ literally, such an interacting fixed point can appear in quasi two dimensional systems. According to experiments [4], these semiconductors are rather anisotropic, where the in-plane resistivity ($\sim 0.001 \Omega cm$) is two-order of magnitude smaller than the out-of-plane one ($\sim 0.1 \Omega cm$), regarded to be quasi two dimensional. In addition, further doping of magnetic impurities is expected to make such magnetically doped semiconductors more isotropic, where the negative longitudinal magnetoresistivity disappears, indeed. It would be important to reveal the distribution pattern of doped magnetic impurities clearly in order to understand the physical meaning of the finiteness of the regularization parameter for our interacting fixed point.

ACKNOWLEDGEMENT

This study was supported by the Ministry of Education, Science, and Technology (No. NRF-2015R1C1A1A01051629 and No. 2011-0030046) of the National Research Foundation of Korea (NRF).

Appendix A: Evaluation of Feynman diagrams

1. Fermion self-energy

The fermion self-energy (1) in Fig. 3 is

$$\begin{aligned}\Sigma(1) &= \sum_{i=1}^d \int \frac{d^{d+\varepsilon_\tau} l}{(2\pi)^{d+\varepsilon_\tau}} (\lambda \gamma_i \gamma_5) G_0(k-l) (\lambda \gamma_i \gamma_5) D_0(l) \\ &= \lambda^2 \sum_i \int \frac{d^{d+\varepsilon_\tau} l}{(2\pi)^{d+\varepsilon_\tau}} \frac{\gamma_i \gamma_5 [-i(\mathbf{k}_\tau - l_\tau) \cdot \boldsymbol{\gamma}_\tau + (\mathbf{k} - l) \cdot \boldsymbol{\gamma} - m] \gamma_i \gamma_5}{[(\mathbf{k}_\tau - l_\tau)^2 + (\mathbf{k} - l)^2 + m^2][l_\tau^2 + c^2 l^2 + r]}.\end{aligned}$$

This can be evaluated in the standard way: Feynman parametrization, a momentum shift, and a spherically-symmetric integration as

$$\begin{aligned}\Sigma(1) &= \lambda^2 \int_0^1 dx \int \frac{d^{d+\varepsilon_\tau} l}{(2\pi)^{d+\varepsilon_\tau}} \frac{-id(\mathbf{k}_\tau - l_\tau) \cdot \boldsymbol{\gamma}_\tau + (d-2)(\mathbf{k} - l) \cdot \boldsymbol{\gamma} - dm}{[(l_\tau - x\mathbf{k}_\tau)^2 + a_x^2(l - x\mathbf{k}/a_x^2)^2 + \Delta]} \\ &= \lambda^2 \int_0^1 dx \int \frac{d^{d+\varepsilon_\tau} \tilde{l}}{(2\pi)^{d+\varepsilon_\tau}} \frac{-id(1-x)\mathbf{k}_\tau \cdot \boldsymbol{\gamma}_\tau + (d-2)(1-x)\frac{c^2}{a_x^2}(\mathbf{k} \cdot \boldsymbol{\gamma}) - dm}{a_x^d[\tilde{l}^2 + \Delta]^2} \\ &= \frac{\lambda^2 \Gamma(\frac{4-d-\varepsilon_\tau}{2})}{(4\pi)^{(d+\varepsilon_\tau)/2}} \int_0^1 dx \frac{-id(1-x)\mathbf{k}_\tau \cdot \boldsymbol{\gamma}_\tau + (d-2)(1-x)\frac{c^2}{a_x^2}(\mathbf{k} \cdot \boldsymbol{\gamma}) - dm}{a_x^d[\Delta]^{\frac{4-d-\varepsilon_\tau}{2}}},\end{aligned}$$

where $\Delta = x(1-x)(\mathbf{k}_\tau^2 + c^2\mathbf{k}^2/a_x^2) + xm^2 + (1-x)r$ and $a_x^2 = x + (1-x)c^2$. In the second line, the loop momentum is scaled as $l \rightarrow l/a_x$ and then redefined as $\tilde{l} = (l_\tau - x\mathbf{k}_\tau, l - x\mathbf{k}/a_x)$.

Near $d = 3$ and $\varepsilon_\tau = 1$, we get

$$\Sigma(1) = \frac{\lambda^2}{8\pi^2\varepsilon}[-i3n_1\mathbf{k}_\tau \cdot \boldsymbol{\gamma}_\tau + n_2\mathbf{k} \cdot \boldsymbol{\gamma} - 3n_3m] + \mathcal{O}(1),$$

where

$$n_1 = \int_0^1 dx \frac{1-x}{d_x^{3/2}} = \frac{2}{c(1+c)^2}, \quad n_2 = \int_0^1 dx \frac{(1-x)c^2}{d_x^{5/2}} = \frac{2(1+2c)}{3c(1+c)^2}, \quad n_3 = \int_0^1 dx \frac{1}{d_x^{3/2}} = \frac{2}{c(1+c)}.$$

Using Eq. (12), we find the counterterms for the fermion dynamics as

$$\delta_0 = -\frac{3\lambda^2}{4\pi^2\varepsilon c(1+c)^2}, \quad \delta_1 = -\frac{(1+2c)\lambda^2}{12\pi^2\varepsilon c(1+c)^2}, \quad \delta_m = +\frac{3\lambda^2}{4\pi^2\varepsilon c(1+c)}. \quad (\text{A1})$$

This result is comparable with that of QED in four dimensions, referred to as QED4. In QED4, we have $\delta_\psi = \frac{e^2(2-d)}{16\pi^2(4-d)} \xrightarrow{d \rightarrow 4} -\frac{e^2}{8\pi^2\varepsilon}$ and $\delta_m = \frac{e^2(-d)}{8\pi^2(4-d)} \xrightarrow{d \rightarrow 4} -\frac{e^2}{2\pi^2\varepsilon}$. Setting $c = 1$ and tracking the dimensional factors, we observe that the above counterterms are reduced into

$$\delta_0 \xrightarrow{d \rightarrow 3} -\frac{3\lambda^2}{16\pi^2\varepsilon}, \quad \delta_1 \xrightarrow{d \rightarrow 3} -\frac{\lambda^2}{16\pi^2\varepsilon}, \quad \delta_m \xrightarrow{d \rightarrow 3} +\frac{3e^2}{8\pi^2\varepsilon}.$$

The Φ -field has three space components but without the time component, so it gives $3/2$, $1/2$, and $-3/4$ factors for the field, the velocity, and the mass counterterm, respectively.

2. Boson self-energy

In Fig. 3, bosons get self-energy corrections (2) from the Zeeman coupling, (3) and (4) from the boson self-interaction, (5) from the disorder scattering, respectively.

a. Zeeman coupling

The correction (2) is

$$\begin{aligned} \Pi_{ii}(2) &= -\lambda^2 \int \frac{d^{d+\varepsilon_\tau}l}{(2\pi)^{d+\varepsilon_\tau}} \text{tr}[\gamma_i \gamma_5 G_0(l+q) \gamma_i \gamma_5 G_0(q)] \\ &= -\lambda^2 \int \frac{d^{d+\varepsilon_\tau}l}{(2\pi)^{d+\varepsilon_\tau}} \frac{4(-l \cdot (l+q) + 2l_i(l_i+q_i) + m^2)}{[(l+q)^2 + m^2][l^2 + m^2]} \\ &= -4\lambda^2 \int_0^1 dx \int \frac{d^{d+\varepsilon_\tau}l}{(2\pi)^{d+\varepsilon_\tau}} \frac{\frac{-d-\varepsilon_\tau+2}{d+\varepsilon_\tau}(l+xq)^2 + x(1-x)(q^2 - 2q_i^2) + m^2}{[(l+xq)^2 + x(1-x)q^2 + m^2]^2} \\ &= -\frac{4\lambda^2}{(4\pi)^{(d+\varepsilon_\tau)/2}} \int_0^1 dx \frac{(2x(1-x)q^2 - 2x(1-x)q_i^2 + 2m^2)\Gamma(\frac{4-d-\varepsilon_\tau}{2})}{[x(1-x)q^2 + m^2]^{\frac{4-d-\varepsilon_\tau}{2}}}. \end{aligned}$$

Near $d = 3$ and $\varepsilon_\tau = 1$, we get

$$\Pi_{ii}(2) = -\frac{\lambda^2(\mathbf{q}_\tau^2 + \mathbf{q}^2 - \mathbf{q}_i^2)}{6\pi^2\varepsilon} - \frac{\lambda^2 m^2}{\pi^2\varepsilon}.$$

b. Boson interaction

The correction (3) is

$$\Pi_{ii}(3) = -\frac{Nu}{2} \int \frac{d^{d+\varepsilon_\tau}l}{(2\pi)^{d+\varepsilon_\tau}} D_0(q-l) = -\frac{Nu}{2} \int \frac{d^{d+\varepsilon_\tau}l}{(2\pi)^{d+\varepsilon_\tau}} \frac{1}{l_\tau^2 + c^2 l^2 + r} = -\frac{Nu\Gamma(\frac{2-d-\varepsilon_\tau}{2})}{2(4\pi)^{(d+\varepsilon_\tau)/2} c d r^{\frac{2-d-\varepsilon_\tau}{2}}}.$$

Near $d = 3$ and $\varepsilon_\tau = 1$, we get $\Pi_{ii}(3) = \frac{Nur}{16\pi^2\varepsilon c^3}$. The correction (4) in the same line is similar except for the absence of the $\frac{N}{2}$ factor. The result is $\Pi_{ii}(4) = \frac{ur}{8\pi^2\varepsilon c^3}$.

c. Disorder scattering

The correction (5) is

$$\Pi_{ii}(5) = \Gamma_m \int \frac{d^{d+\varepsilon_\tau} l}{(2\pi)^d} D_0(q-l) \delta^{(\varepsilon_\tau)}(l_\tau) = \Gamma_m \int \frac{d^d l}{(2\pi)^d} \frac{1}{c^2 l^2 + \mathbf{q}_\tau^2 + r} = \frac{\Gamma_m \Gamma(\frac{2-d}{2})}{(4\pi)^{d/2} c^d (\mathbf{q}_\tau^2 + r)^{\frac{2-d}{2}}}.$$

Near $d = 3$ and $\varepsilon_\tau = 1$, we get $\Pi_{ii}(5) = -\frac{4\Gamma_m(\mathbf{q}_\tau^2 + r)}{(4\pi)^{3/2}(\varepsilon + \varepsilon_\tau)c^3}$.

d. Counterterms

The total boson self-energy is

$$\begin{aligned} \Pi_{ii}(q) &= \Pi_{ii}(2) + \Pi_{ii}(3) + \Pi_{ii}(4) + \Pi_{ii}(5) \\ &= -\frac{\lambda^2(\mathbf{q}_\tau^2 + \mathbf{q}^2 - \mathbf{q}_i^2)}{6\pi^2\varepsilon} - \frac{\lambda^2 m^2}{\pi^2\varepsilon} + \frac{(N+2)ur}{16\pi^2\varepsilon c^3} - \frac{4\Gamma_m(\mathbf{q}_\tau^2 + r)}{(4\pi)^{3/2}(\varepsilon + \varepsilon_\tau)c^3}. \end{aligned}$$

The Zeeman coupling term results in two unusual features and their corresponding complications. First, it has a transverse-mode structure ($\Pi_{ii} \sim \mathbf{q}^2 - \mathbf{q}_i^2$) while the original action doesn't. This is not surprising because bosons are coupled to Dirac fermions in the fashion of the “gauge field” (chiral). However, we'll just ignore \mathbf{q}_i^2 to find the counterterms by assuming that the effective action is “chosen” for the Feynman gauge so that no projection appears in Eq. (7). Second, a mass-shift proportional to the fermion mass appears. This makes the boson mass increase even at the critical point. Thus, in a naive view point, there is no critical state. Recall that the similar thing happens in the ϕ^4 -theory with a cutoff (Λ), where a mass shift proportional to Λ^2 appears. Redefinition of the boson mass with including the shift is required to access the critical point. Practically, this can be done by eliminating the additional mass shift. We'll do the same thing here: the mass shift is canceled by an ad hoc counterterm, not participating in the renormalization group.

Based on the above discussion, we find the counterterms for the bosons as

$$\delta_2 = -\frac{\lambda^2}{6\pi^2\varepsilon} - \frac{4\Gamma_m}{(4\pi)^{3/2}(\varepsilon + \varepsilon_\tau)c^3}, \quad \delta_c = -\frac{\lambda^2}{6\pi^2\varepsilon c^2}, \quad \delta_r = \frac{(N+2)u}{16\pi^2\varepsilon c^3} - \frac{4\Gamma_m}{(4\pi)^{3/2}(\varepsilon + \varepsilon_\tau)c^3}. \quad (\text{A2})$$

Compared with the result of QED4, $\delta_A = -\frac{e^2}{6\pi^2\varepsilon}$, the counterterms have the same numerical factor. However, due to the presence of velocity factors, c gets renormalized for the fermion velocity $v = 1$. Actually, this renormalization structure appears ubiquitously [19] at least in the models that critical bosons are coupled to Dirac fermions.

3. Vertex corrections

The boson self-interaction and the disorder scattering can be mixed, while the Zeeman coupling gets affected from the others only through the field renormalization. We calculate the disorder scattering, the boson interaction, mixing of them, and the Zeeman coupling in turn.

a. Disorder scattering

We calculate the diagrams of (1), (2), and (3) in Fig. 4. The correction (1) is

$$\begin{aligned} \delta\Gamma_m(1) &= \Gamma_m^2 \int \frac{d^{d+\varepsilon_\tau} l}{(2\pi)^{d+\varepsilon_\tau}} D_0(k+l) D_0(k'-l) (2\pi)^{\varepsilon_\tau} \delta^{(\varepsilon_\tau)}(l_\tau) \\ &= \frac{\Gamma_m^2}{c^d} \int_0^1 dx \int \frac{d^{d+\varepsilon_\tau} l}{(2\pi)^{d+\varepsilon_\tau}} \frac{(2\pi)^{\varepsilon_\tau} \delta^{(\varepsilon_\tau)}(l_\tau)}{[(l+xk+(1-x)k')^2 + x(1-x)(k-k')^2 + r]^2} \\ &= \frac{\Gamma_m^2}{c^d} \int_0^1 dx \int \frac{d^d l}{(2\pi)^d} \frac{1}{[(l+x\mathbf{k}+(1-x)\mathbf{k}')^2 + \Delta]^2} \\ &= \frac{\Gamma_m^2}{(4\pi)^{d/2} c^d} \int_0^1 dx \frac{\Gamma(\frac{4-d}{2})}{[\Delta]^{\frac{4-d}{2}}}, \end{aligned}$$

where $\Delta = (x\mathbf{k}_\tau + (1-x)\mathbf{k}'_\tau)^2 + x(1-x)(k-k')^2 + r$. Near $d = 3$ and $\varepsilon_\tau = 1$, we find $\delta\Gamma_m(1) = \frac{2\Gamma_m^2}{(4\pi)^{3/2}c^3(\varepsilon+\varepsilon_\tau)}$. Other corrections differ from this only with numerical factors. The correction (2) is the same. The correction (3) is two times larger because there are two inequivalent diagrams. As a result, we find

$$\delta\Gamma_m(1) = \frac{2\Gamma_m^2}{(4\pi)^{3/2}c^3(\varepsilon+\varepsilon_\tau)}, \quad \delta\Gamma_m(2) = \frac{2\Gamma_m^2}{(4\pi)^{3/2}c^3(\varepsilon+\varepsilon_\tau)}, \quad \delta\Gamma_m(3) = \frac{4\Gamma_m^2}{(4\pi)^{3/2}c^4(\varepsilon+\varepsilon_\tau)}. \quad (\text{A3})$$

b. Boson interaction

We calculate the diagrams of (6), (7), (8), and (9) in Fig. 4. The correction (6) is

$$\begin{aligned} \delta u(6) &= u^2 \int \frac{d^{d+\varepsilon_\tau}l}{(2\pi)^{d+\varepsilon_\tau}} D_0(q+l)D_0(l) = \frac{u^2}{c^d} \int \frac{d^{d+\varepsilon_\tau}l}{(2\pi)^{d+\varepsilon_\tau}} \frac{1}{((q+l)^2+r)(l^2+r)} \\ &= \frac{u^2}{c^d} \int_0^1 dx \int \frac{d^{d+\varepsilon_\tau}l}{(2\pi)^{d+\varepsilon_\tau}} \frac{1}{[(l+xq)^2+\Delta]^2} = \frac{u^2}{(4\pi)^{\frac{d+\varepsilon_\tau}{2}}c^d} \int_0^1 dx \frac{\Gamma(\frac{4-d-\varepsilon_\tau}{2})}{[\Delta]^{\frac{4-d-\varepsilon_\tau}{2}}}, \end{aligned}$$

where $\Delta = x(1-x)q^2 + r$. We find $\delta u(6) = \frac{u^2}{8\pi^2\varepsilon c^3}$. The other corrections can be found similarly. The correction (7) is the same. The correction (8) is two times larger because there are two inequivalent diagrams. The correction (9) is $\frac{N}{2}$ times the first correction, where 2 comes from two equivalent vertices and N results from a free index summation. As a result, we find

$$\delta u(6) = \frac{u^2}{8\pi^2\varepsilon c^3}, \quad \delta u(7) = \frac{u^2}{8\pi^2c^3\varepsilon}, \quad \delta u(8) = \frac{u^2}{4\pi^2c^3\varepsilon}, \quad \delta u(9) = \frac{Nu^2}{16\pi^2c^3\varepsilon}. \quad (\text{A4})$$

c. Mixing of boson interaction and disorder scattering

The disorder scattering gets corrections from the diagrams of (4) and (5) in Fig. 4. The calculation of (4) is similar with that of (1) because frequency is not exchanged in the loop. Numerical factor is $2N$, where 2 comes from two inequivalent diagrams and N results from a free index summation. The calculation of (5) is similar with that of (6) because frequency is exchanged in this case. Numerical factor is 2 because there are two inequivalent diagrams. As a result, we find

$$\delta\Gamma_m(4) = -\frac{4Nu\Gamma_m}{(4\pi)^{3/2}c^3(\varepsilon+\varepsilon_\tau)}, \quad \delta\Gamma_m(5) = -\frac{u\Gamma_m}{4\pi^2c^3\varepsilon}. \quad (\text{A5})$$

The boson interaction gets corrections from the diagrams of (10), (11), and (12). The calculations are similar with that of (1) because frequency is not exchanged. Numerical factors are 2 because there are two inequivalent diagrams. As a result, we find

$$\delta u(10) = -\frac{4u\Gamma_m}{(4\pi)^{3/2}c^3(\varepsilon+\varepsilon_\tau)}, \quad \delta u(11) = -\frac{4u\Gamma_m}{(4\pi)^{3/2}c^3(\varepsilon+\varepsilon_\tau)}, \quad \delta u(12) = -\frac{4u\Gamma_m}{(4\pi)^{3/2}c^3(\varepsilon+\varepsilon_\tau)}. \quad (\text{A6})$$

d. Zeeman coupling term

The correction (14) in Fig. 4 is

$$\begin{aligned} \delta\lambda(14)\gamma_i\gamma_5 &= \sum_{j=1}^3 \int \frac{d^{d+\varepsilon_\tau}l}{(2\pi)^{d+\varepsilon_\tau}} D_0(p-l)(\lambda\gamma_j\gamma_5)G_0(l+q)(\lambda\gamma_i\gamma_5)G_0(l)(\lambda\gamma_j\gamma_5) \\ &= \lambda^3 \sum_j \int \frac{d^{d+\varepsilon_\tau}l}{(2\pi)^{d+\varepsilon_\tau}} \frac{\gamma_j\gamma_5[-i(l_\tau+\mathbf{q}_\tau)\cdot\boldsymbol{\gamma}_\tau+(l+\mathbf{q})\cdot\boldsymbol{\gamma}-m]\gamma_i\gamma_5}{[l_\tau^2+l^2+m^2][(p_\tau-l_\tau)^2+c^2(p-l)^2+r]} \\ &\quad \times \frac{[-il_\tau\cdot\boldsymbol{\gamma}_\tau+l\cdot\boldsymbol{\gamma}-m]\gamma_j\gamma_5}{[(p_\tau-l_\tau)^2+c^2(p-l)^2+r][(l_\tau+\mathbf{q}_\tau)^2+(l+\mathbf{q})^2+m^2]}. \end{aligned}$$

This is rearranged as

$$\delta\lambda(14)\gamma_i\gamma_5 = \lambda^3 \int_0^1 dx dy dz \delta(1-x-y-z) \int \frac{d^{d+\varepsilon_\tau} \tilde{l}}{(2\pi)^{d+\varepsilon_\tau}} \frac{2\mathcal{N}}{\mathcal{D}^3},$$

where

$$\begin{aligned} \mathcal{D} &= \tilde{l}_\tau^2 + a_x^2 \tilde{l}^2 + \Delta, \\ \tilde{l} &= (l_\tau - x\mathbf{p}_\tau + y\mathbf{q}_\tau, l - (xc^2/a_x^2)\mathbf{p} + (y/a_x^2)\mathbf{q}), \\ \Delta &= x(1-x)\mathbf{p}_\tau^2 + y(1-y)\mathbf{q}_\tau^2 + 2xy\mathbf{p}_\tau \cdot \mathbf{q}_\tau \\ &\quad + (xyc^2(\mathbf{p} + \mathbf{q})^2 + xzc^2\mathbf{p}^2 + yz\mathbf{q}^2)/a_x^2 + xr + (1-x)m^2, \\ a_x^2 &= xc^2 + (1-x). \end{aligned} \tag{A7}$$

The numerator is given by

$$\begin{aligned} \mathcal{N} &= \sum_j \gamma_j \gamma_5 [-i(l_\tau + \mathbf{q}_\tau) \cdot \gamma_\tau + (l + \mathbf{q}) \cdot \gamma - m] \gamma_i \gamma_5 [l_\tau \cdot \gamma_\tau + l \cdot \gamma - m] \gamma_j \gamma_5 \\ &= \sum_j \gamma_j \gamma_5 [-i\tilde{l}_\tau \cdot \gamma_\tau + \tilde{l} \cdot \gamma] \gamma_i \gamma_5 [-i\tilde{l}_\tau \cdot \gamma_\tau + \tilde{l} \cdot \gamma] \gamma_j \gamma_5 + \mathcal{O}(\tilde{l}) \\ &\rightarrow [(d-2)\tilde{l}_\tau^2 + (d-2)^2\tilde{l}_k^2] \gamma_i \gamma_5. \end{aligned}$$

In the last line, only the quadratic terms are kept.

The integration is straightforward, and the result is

$$\delta\lambda(14) = \lambda^3 \int_0^1 dx dy dz \delta(1-x-y-z) \frac{\Gamma(\frac{4-d-\varepsilon_\tau}{2})[(d-2) + (d-2)^2/a_x^2]}{a_x^d 2(4\pi)^{(d+1)/2} \Delta^{\frac{4-d-\varepsilon_\tau}{2}}}.$$

Near $d = 3$ and $\varepsilon_\tau = 1$, we find

$$\delta\lambda(14) = \frac{\lambda^3}{16\pi^2\varepsilon} \int_0^1 dx dy dz \delta(1-x-y-z) (a_x^{-3} + a_x^{-5}) = \frac{\lambda^3(1+2c)}{12\pi^2\varepsilon c(1+c)^2}. \tag{A8}$$

Lastly, we calculate the correction (13). It should be interpreted as an amputated diagram since six distinct diagrams appear when it is contracted to external lines. It possibly gives a correction for the boson interaction because a power counting tells that it may have a logarithmic divergence. However, it turns out not to diverge.

The correction (13) is

$$\begin{aligned} \delta u(13) &= -\lambda^4 \int \frac{d^{d+\varepsilon_\tau} l}{(2\pi)^{d+\varepsilon_\tau}} \text{tr}[\gamma_i \gamma_5 G_0(l) \gamma_j \gamma_5 G_0(l+k) \gamma_k \gamma_5 G_0(l-q) \gamma_l \gamma_5 G_0(l-k')] \\ &= -\lambda^4 \int_0^1 dx dy dz dw \int \frac{d^{d+\varepsilon_\tau} l}{(2\pi)^{d+\varepsilon_\tau}} \delta(1-x-y-z-w) \frac{3!\mathcal{N}}{\mathcal{D}^4}. \end{aligned}$$

The denominator and the numerator are

$$\begin{aligned} \mathcal{D} &= (l + yk - zq - wk')^2 + \Delta, \\ \Delta &= y(1-y)k^2 + z(1-z)q^2 + w(1-w)k'^2 + 2(yzk \cdot q - zwq \cdot k' + ywk \cdot k'), \\ \mathcal{N} &= \text{tr}[\gamma_i \gamma_5 (l \cdot \gamma) \gamma_j \gamma_5 ((l+k) \cdot \gamma) \gamma_k \gamma_5 ((l-q) \cdot \gamma) \gamma_l \gamma_5 ((l-k') \cdot \gamma)] \\ &\rightarrow \text{tr}[\gamma_i \gamma_5 \tilde{l} \cdot \gamma \gamma_j \gamma_5 \tilde{l} \cdot \gamma \gamma_k \gamma_5 \tilde{l} \cdot \gamma \gamma_l \gamma_5 \tilde{l} \cdot \gamma], \end{aligned}$$

where $\tilde{l} = l + yk - zq - wk'$ and only the quartic term is kept in the last line.

The integration is straightforward and the result is

$$\begin{aligned} \delta u(13) &= -\frac{\lambda^4 \Gamma(\frac{4-d-\varepsilon_\tau}{2})}{(4\pi)^{(d+\varepsilon_\tau)/2}} \int_0^1 dx dy dz dw \frac{\delta(1-x-y-z-w)}{[\Delta]^{\frac{4-d-\varepsilon_\tau}{2}}} \\ &\quad \times \frac{1}{4} (\delta_{\mu\nu} \delta_{\rho\sigma} + \delta_{\mu\rho} \delta_{\nu\sigma} + \delta_{\mu\sigma} \delta_{\nu\rho}) \text{tr}[\gamma_i \gamma_5 \gamma_\mu \gamma_j \gamma_5 \gamma_\nu \gamma_k \gamma_5 \gamma_\rho \gamma_l \gamma_5 \gamma_\sigma]. \end{aligned}$$

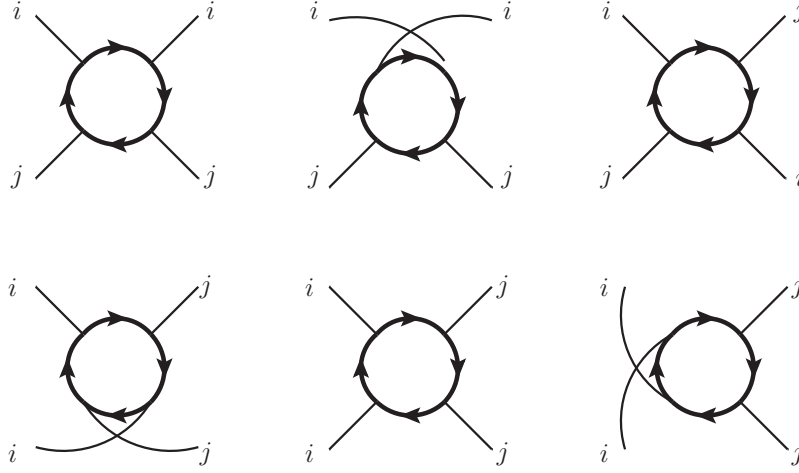


FIG. 9: Vertex corrections for the boson interaction from the four Zeeman couplings. Three diagrams in the first line are \mathcal{M}_1 , \mathcal{M}_2 , and \mathcal{M}_3 from left to right, and three diagrams in the second, \mathcal{M}_4 , \mathcal{M}_5 , and \mathcal{M}_6 .

Near $d = 3$ and $\varepsilon_\tau = 1$, we find

$$\delta u(13) = -\frac{\lambda^4}{192\pi^2\varepsilon}(\delta_{\mu\nu}\delta_{\rho\sigma} + \delta_{\mu\rho}\delta_{\nu\sigma} + \delta_{\mu\sigma}\delta_{\nu\rho})\text{tr}[\gamma_i\gamma_\mu\gamma_j\gamma_\nu\gamma_k\gamma_\rho\gamma_l\gamma_\sigma],$$

where we used $\int_0^1 dx dy dz dw \delta(1-x-y-z-w) = \frac{1}{6}$.

Taking the trace, we have

$$\begin{aligned}\text{tr}[\gamma_i\gamma_\mu\gamma_j\gamma_\nu\gamma_k\gamma_l\gamma_\nu] &= \text{tr}[\gamma_i\gamma_\mu\gamma_j\gamma_\nu\gamma_k\gamma_l\gamma_\mu] \simeq 16(\delta_{ij}\delta_{kl} - \delta_{ik}\delta_{jl} + \delta_{il}\delta_{jk}), \\ \text{tr}[\gamma_i\gamma_\mu\gamma_j\gamma_\nu\gamma_k\gamma_l\gamma_\nu] &= -32\delta_{ik}\delta_{jl},\end{aligned}$$

where $\mathcal{O}(\varepsilon)$ terms are dropped. In the calculation, we used the following identities repeatedly:

$$\begin{aligned}\gamma_\mu\gamma_\nu\gamma_\mu &= (d-2+\varepsilon_\tau)\gamma_\nu, \\ \gamma_\mu\gamma_\nu\gamma_\rho\gamma_\mu &= 4\delta_{\nu\rho} - (d-4+\varepsilon_\tau)\gamma_\nu\gamma_\rho, \\ \gamma_\mu\gamma_\nu\gamma_\rho\gamma_\sigma\gamma_\mu &= 2\gamma_\sigma\gamma_\rho\gamma_\nu + (d-4+\varepsilon_\tau)\gamma_\nu\gamma_\rho\gamma_\sigma.\end{aligned}$$

As a result, we find

$$\delta u(13) = -\frac{\lambda^4}{6\pi^2\varepsilon}(\delta_{ij}\delta_{kl} - 2\delta_{ik}\delta_{jl} + \delta_{il}\delta_{jk}).$$

Contracted to external fields, each gives rise to two diagrams because there are four options but each two are the same. See Fig. 9. As a result, we obtain

$$\mathcal{M}_1 = \mathcal{M}_2 = \mathcal{M}_3 = \mathcal{M}_4 = -\frac{\lambda^4}{6\pi^2\varepsilon}, \quad \mathcal{M}_5 = \mathcal{M}_6 = \frac{\lambda^4}{3\pi^2\varepsilon}.$$

Note that their sum is zero $\sum_{i=1}^6 \mathcal{M}_i = 0$. Thus, its logarithmic divergence is cancelled as well known in the Ward identity of QED4.

e. Counterterms

We gather all the results from Eqs. (A3), (A4), (A5), (A6), and (A8) as

$$\begin{aligned}\sum_{i=1}^5 \delta\Gamma_m(i) &= \frac{8\Gamma_m^2 - 4Nu\Gamma_m}{(4\pi)^{3/2}c^3(\varepsilon + \varepsilon_\tau)} - \frac{u\Gamma_m}{4\pi^2c^3\varepsilon} - \frac{4Nu\Gamma_m}{(4\pi)^{3/2}c^3(\varepsilon + \varepsilon_\tau)}, \\ \sum_{i=6}^{12} \delta u(i) &= \frac{(N+8)u^2}{16\pi^2c^3\varepsilon} - \frac{12u\Gamma_m}{(4\pi)^{3/2}c^3(\varepsilon + \varepsilon_\tau)}, \quad \sum_{i=14}^{14} \delta\lambda(i) = \frac{\lambda^3(1+2c)}{12\pi^2c(1+c)^2\varepsilon}.\end{aligned}$$

Using Eq. (12), we find

$$\begin{aligned}\delta\Gamma_m &= -\frac{8\Gamma_m}{(4\pi)^{3/2}c^3(\varepsilon + \varepsilon_\tau)} + \frac{u}{4\pi^2c^3\varepsilon} + \frac{4Nu}{(4\pi)^{3/2}c^3(\varepsilon + \varepsilon_\tau)}, \\ \delta_u &= \frac{(N+8)u}{16\pi^2c^3\varepsilon} - \frac{12\Gamma_m}{(4\pi)^{3/2}c^3(\varepsilon + \varepsilon_\tau)}, \quad \delta_\lambda = -\frac{\lambda^2(1+2c)}{12\pi^2c(1+c)^2\varepsilon}.\end{aligned}\tag{A9}$$

Appendix B: Ward identity

In the one-loop order, the Ward identity is satisfied, i.e., $Z_1 = Z_\lambda$. This is rather unexpected in the respect that the chiral symmetry is *already broken* by the mass term in the classical level. However, the result turns out to be consistent as will be shown in this section.

We focus on $S_f = \int dx \bar{\psi}(x)(i\partial_\mu\gamma_\mu + m)\psi(x)$, where $\partial_\mu = (-i\partial_0, \partial_r)$ and $\gamma_\mu = (\gamma_0, \gamma)$. Performing the chiral transformation given by

$$\psi(x) \rightarrow e^{i\alpha(x)\gamma_5}\psi(x),\tag{B1}$$

we have

$$\delta S_f = \int dx \{ \partial_\mu \alpha(x) \bar{\psi}(x) \gamma_\mu \gamma_5 \psi(x) + 2im\alpha(x) \bar{\psi}(x) \gamma_5 \psi(x) \}.\tag{B2}$$

Thus, the action is not invariant not only by the chiral current term but also by the pseudo-scalar term proportional to the mass.

We calculate the fermion Green's function:

$$\langle \psi(x_1) \bar{\psi}(x_2) \rangle = \frac{1}{\mathcal{Z}} \int \mathcal{D}(\bar{\psi}, \psi) \psi(x_1) \bar{\psi}(x_2) e^{-S},\tag{B3}$$

where $\mathcal{Z} = \int \mathcal{D}(\bar{\psi}, \psi) e^{-S}$. If we assume Eq. (B3) is invariant by Eq. (B1) in spite of the explicit symmetry breaking, we have

$$\begin{aligned}0 &= - \int dx \{ \partial_\mu \alpha(x) \bar{\psi}(x) \gamma_\mu \gamma_5 \psi(x) + 2im\alpha(x) \bar{\psi}(x) \gamma_5 \psi(x) \} \psi(x_1) \bar{\psi}(x_2) \\ &\quad + i\alpha(x_1) \langle \gamma_5 \psi(x_1) \bar{\psi}(x_2) \rangle + i\alpha(x_2) \langle \psi(x_1) \bar{\psi}(x_2) \gamma_5 \rangle + \mathcal{O}(\alpha^2) \\ &= \int dx \alpha(x) \{ \partial_\mu \langle \bar{\psi}(x) \gamma_\mu \gamma_5 \psi(x) \psi(x_1) \bar{\psi}(x_2) \rangle + 2im \langle \bar{\psi}(x) \gamma_5 \psi(x) \psi(x_1) \bar{\psi}(x_2) \rangle \\ &\quad + i\delta(x-x_1) \langle \gamma_5 \psi(x_1) \bar{\psi}(x_2) \rangle + i\delta(x-x_2) \langle \psi(x_1) \bar{\psi}(x_2) \gamma_5 \rangle \} + \mathcal{O}(\alpha^2),\end{aligned}\tag{B4}$$

where we performed integration by parts on $\partial_\mu \alpha(x)$ and used $\alpha(x_1) = \int dx \delta(x-x_1) \alpha(x)$.

The right hand side of Eq. (B4) should be zero order by order. In the one loop order, we have

$$\begin{aligned}&\int dp_1 \{ k_\mu \langle \bar{\psi}(p_1+k) \gamma_\mu \gamma_5 \psi(p_1) \psi(q) \bar{\psi}(p) \rangle - 2m \langle \bar{\psi}(p_1+k) \gamma_5 \psi(p_1) \psi(q) \bar{\psi}(p) \rangle \} \\ &= \langle \gamma_5 \psi(q-k) \bar{\psi}(p) \rangle + \langle \psi(q) \bar{\psi}(p+k) \gamma_5 \rangle.\end{aligned}$$

More compactly, we have

$$k_\mu G(p+k) \Gamma_{\mu 5}(p+k, p) G(p) - 2m G(p+k) \Gamma_5(p+k, p) G(p) = \gamma_5 G(p) + G(p+k) \gamma_5,$$

where $\Gamma_{\mu 5}(p+k, p)$ is the one-particle irreducible vertex for $\int dp_1 \langle \bar{\psi}(p_1+k) \gamma_\mu \gamma_5 \psi(p_1) \psi(q) \bar{\psi}(p) \rangle$ and $\Gamma_5(p+k, p)$ is that for $\int dp_1 \langle \bar{\psi}(p_1+k) \gamma_5 \psi(p_1) \psi(q) \bar{\psi}(p) \rangle$.

Multiplying $G^{-1}(p+k)$ on the left and $G^{-1}(p)$ on the right, we have

$$k_\mu \Gamma_{\mu 5}(p+k, p) = G^{-1}(p+k) \gamma_5 + \gamma_5 G^{-1}(p) + 2m \Gamma_5(p+k, p).$$

Recalling $G^{-1}(p) = Z_0 i \mathbf{p}_\tau \cdot \boldsymbol{\gamma}_\tau - Z_1 \mathbf{p} \cdot \boldsymbol{\gamma} - Z_m m$, we find $\gamma_5 G^{-1}(p) = -G^{-1}(p) \gamma_5 - 2Z_m m \gamma_5$.

Resorting to this expression, we obtain

$$k_\mu \Gamma_{\mu 5}(p+k, p) = G^{-1}(p+k) \gamma_5 - G^{-1}(p) \gamma_5 + 2m(Z_5 - Z_m) \gamma_5,$$

where $Z_5\gamma_5 \equiv \lim_{k \rightarrow 0} \Gamma_5(p+k, p)$. If $Z_5 = Z_m$, we have the Ward identity:

$$Z_{\mu 5} \gamma_\mu \gamma_5 \equiv \lim_{k \rightarrow 0} \Gamma_{\mu 5}(p+k, p) \stackrel{!}{=} \frac{\partial G^{-1}(p)}{\partial p_\mu} \gamma_5. \quad (\text{B5})$$

In order to verify Eq. (B5), we calculate Z_5 . It given by

$$\begin{aligned} \delta\Gamma_5\gamma_5 &= \sum_{j=1}^3 \int \frac{d^{d+\varepsilon_\tau} l}{(2\pi)^{d+\varepsilon_\tau}} D_0(p-l)(\lambda\gamma_j\gamma_5)G_0(l+q)(\gamma_5)G_0(l)(\lambda\gamma_j\gamma_5) \\ &= \lambda^2 \sum_j \int \frac{d^{d+\varepsilon_\tau} l}{(2\pi)^{d+\varepsilon_\tau}} \frac{\gamma_j\gamma_5[-i(l_\tau + \mathbf{q}_\tau) \cdot \boldsymbol{\gamma}_\tau + (l + \mathbf{q}) \cdot \boldsymbol{\gamma} - m]\gamma_5}{[(\mathbf{p}_\tau - l_\tau)^2 + c^2(\mathbf{p} - l)^2 + r]} \\ &\quad \times \frac{[-il_\tau \cdot \boldsymbol{\gamma}_\tau + l \cdot \boldsymbol{\gamma} - m]\gamma_j\gamma_5}{[(l_\tau + \mathbf{q}_\tau)^2 + (l + \mathbf{q})^2 + m^2][l_\tau^2 + l^2 + m^2]}. \end{aligned}$$

This is rearranged as

$$\delta\Gamma_5\gamma_5 = \lambda^2 \int_0^1 dx dy dz \delta(1-x-y-z) \int \frac{d^{d+\varepsilon_\tau} \tilde{l}}{(2\pi)^{d+\varepsilon_\tau}} \frac{2\mathcal{N}}{\mathcal{D}^3},$$

where \mathcal{D} , \tilde{l} , Δ , and a_x^2 are given in Eq. (A7). The numerator is

$$\begin{aligned} \mathcal{N} &= \sum_j \gamma_j\gamma_5[-i(l_\tau + \mathbf{q}_\tau) \cdot \boldsymbol{\gamma}_\tau + (l + \mathbf{q}) \cdot \boldsymbol{\gamma} - m]\gamma_5[l_\tau \cdot \boldsymbol{\gamma}_\tau + l \cdot \boldsymbol{\gamma} - m]\gamma_j\gamma_5 \\ &= \sum_j \gamma_j\gamma_5[-i\tilde{l}_\tau \cdot \boldsymbol{\gamma}_\tau + \tilde{l} \cdot \boldsymbol{\gamma}]\gamma_5[-i\tilde{l}_\tau \cdot \boldsymbol{\gamma}_\tau + \tilde{l} \cdot \boldsymbol{\gamma}]\gamma_j\gamma_5 + \mathcal{O}(\tilde{l}) \\ &\rightarrow -d[\tilde{l}_\tau^2 + \tilde{l}^2]\gamma_i\gamma_5. \end{aligned}$$

In the last line, only the quadratic terms are kept.

The integration is straightforward, and the result is

$$\delta\Gamma_5 = -\lambda^2 \int_0^1 dx dy dz \delta(1-x-y-z) \frac{\Gamma(\frac{4-d-\varepsilon_\tau}{2})[d + d^2/a_x^2]}{a_x^d 2(4\pi)^{(d+1)/2} \Delta^{\frac{4-d-\varepsilon_\tau}{2}}}.$$

Near $d = 3$ and $\varepsilon_\tau = 1$, we find

$$\delta\Gamma_5 = -\frac{\lambda^2}{16\pi^2\epsilon} \int_0^1 dx dy dz \delta(1-x-y-z) (3a_x^{-3} + 9a_x^{-5}) = -\frac{3\lambda^2}{4\pi^2\epsilon c(1+c)}. \quad (\text{B6})$$

This is the same with δ_m in Eq. (A1), i.e., $Z_5 = Z_m$. Thus, the Ward identity in Eq. (B5) is proven.

Appendix C: Fixed point structure

The beta functions are given by

$$\begin{aligned} \beta_\alpha &= \alpha[-\varepsilon + f_2(c)\alpha + 2\tilde{\Gamma}], \\ \beta_{\tilde{u}} &= \tilde{u}[-\varepsilon + 11\tilde{u} + f_3(c)\alpha - 5\tilde{\Gamma}], \\ \beta_{\tilde{\Gamma}} &= \tilde{\Gamma}[-1 - \varepsilon - 3\tilde{\Gamma} + f_4(c)\alpha + 4(6\sqrt{\pi} + 1)\tilde{u}], \\ \beta_m &= m[-1 + f_5(c)\alpha], \\ \beta_c &= c[-f_1(c)\alpha + \tilde{\Gamma}], \\ \beta_r &= r[-2 + f_2(c)\alpha + 5\tilde{u}], \end{aligned} \quad (\text{C1})$$

where $\alpha \equiv \frac{\lambda^2}{12\pi^2}$, $\tilde{u} \equiv \frac{u}{16\pi^2 c^3}$, $\tilde{\Gamma} \equiv \frac{2\Gamma_m}{(4\pi)^{3/2} c^3}$, and

$$\begin{aligned} f_1(c) &= -\frac{c^4 + 2c^3 + 2c^2 - 10c - 1}{c^2(1+c)^2}, \quad f_2(c) = \frac{2c^3 + 4c^2 + 4c - 8}{c(1+c)^2}, \\ f_3(c) &= \frac{3+c^2}{c^2}, \quad f_4(c) = \frac{c^4 + 2c^3 + 6c^2 - 2c + 3}{c^2(1+c)^2}, \quad f_5(c) = \frac{10+11c}{c(1+c)^2}. \end{aligned} \quad (\text{C2})$$

α_*	\tilde{u}_*	$\tilde{\Gamma}_*$	c_*	stability
0	0	0	non-universal	unstable
0	$\frac{\varepsilon}{11}$	0	non-universal	unstable
0	0	$-\frac{\varepsilon+1}{3}$	0	unphysical (negative $\tilde{\Gamma}$)
0	$\frac{5+2\varepsilon}{120\sqrt{\pi}-13}$	$\frac{11+\varepsilon(7-24\sqrt{\pi})}{120\sqrt{\pi}-13}$	∞	stable when $0 \leq \varepsilon < 0.08318$
$\frac{\varepsilon}{f_2}$	0	0	$f_1^{-1}(0)$	unphysical (stable when $\varepsilon > 4.055$)
$\frac{\varepsilon}{f_2}$	$\frac{\varepsilon(1-f_3/f_2)}{11} < 0$	0	$f_1^{-1}(0)$	unphysical (negative \tilde{u})
$\frac{5\varepsilon+2}{3f_2+2f_3}$	0	$\frac{\varepsilon f_3 - (\varepsilon+1)f_2}{3f_2+2f_3} < 0$	$[(5\varepsilon+2)f_1 + (\varepsilon+1)f_2 - \varepsilon f_3]^{-1}(0)$	unphysical (negative $\tilde{\Gamma}$)
$\frac{\varepsilon}{2f_1+f_2}$	$\frac{\varepsilon[7f_1+f_2-f_3]}{11[2f_1+f_2]}$	$\frac{\varepsilon f_1}{2f_1+f_2}$	$[\frac{11(5f_1+f_2-f_3)-4(6\sqrt{\pi}+1)[7f_1+f_2-f_3]}{11(2f_1+f_2)}]^{-1}(-\frac{1}{\varepsilon})$	exists and stable when $0.08318 \leq \varepsilon < 0.3103$

TABLE I: All fixed points in the one-loop order are shown.

There are two stable fixed points. The first fixed point (FP1) is

$$\alpha_* = 0, \quad \tilde{u}_* = \frac{5+2\varepsilon}{120\sqrt{\pi}-13}, \quad \tilde{\Gamma}_* = \frac{11+\varepsilon(7-24\sqrt{\pi})}{120\sqrt{\pi}-13}, \quad c_* = 0, \quad (C3)$$

where it is stable when $0 \leq \varepsilon < 0.08318$. All coupling constants are zero but the ratios of the boson interaction and the disorder strength to the boson velocity are finite. This results from the fact that the screening effect of the disorder strength is so strong ($\tilde{\Gamma}_* > \varepsilon/2$) that the Zeeman coupling cannot have a non-Gaussian fixed point ($\beta_\lambda < 0$). The disorder strength makes the boson velocity decrease ($\beta_c \propto -c\tilde{\Gamma}_*$). Since the boson velocity goes to zero, the ratios of $\tilde{u} \sim u/c^3$ and $\tilde{\Gamma} \sim \Gamma_m/c^3$ are finite.

The anomalous dimensions are given by

$$z = 1, \quad \eta_\psi = 0, \quad \eta_\Phi = 0.0551 - 0.178\varepsilon, \quad \nu_m^{-1} = 1, \quad \nu_r^{-1} = 1.96 - 0.805\varepsilon. \quad (C4)$$

Note that the scaling law of fermions is trivial: $z = 1$, $\eta_\psi = 0$, and $\nu_m = 1$. This is because fermions are non-interacting ($\lambda \rightarrow 0$) in the low energy limit. On the other hand, the interaction strength and the disorder strength change the scaling law of bosons: $\eta_\phi \neq 0$ and $\nu_r \neq 0.5$. Thus, this phase is rather trivial in that it is thought to be a Wilson-Fisher fixed point with a finite disorder strength.

The second fixed point (FP2) is

$$\alpha_* = \frac{\varepsilon}{2f_1(c_*) + f_2(c_*)}, \quad \tilde{u}_* = \frac{\varepsilon[7f_1(c_*) + f_2(c_*) - f_3(c_*)]}{11[2f_1(c_*) + f_2(c_*)]}, \quad \tilde{\Gamma}_* = \frac{\varepsilon f_1(c_*)}{2f_1(c_*) + f_2(c_*)},$$

$$\frac{5f_1(c_*) + f_2(c_*) - f_4(c_*)}{2f_1(c_*) + f_2(c_*)} - \frac{4(6\sqrt{\pi}+1)}{11} \frac{7f_1(c_*) + f_2(c_*) - f_3(c_*)}{2f_1(c_*) + f_2(c_*)} = -\frac{1}{\varepsilon}, \quad (C5)$$

where c_* is obtained by solving the last equation. Numerically, the second fixed point is given by

$$\lambda_* = 6.897 + 2.446 \ln \varepsilon, \quad u_* = 4.052 + 0.7732\varepsilon,$$

$$\Gamma_{m*} = 1.031 + 2.450\varepsilon, \quad c_* = 1.367 - 0.02158\varepsilon^{-1.5}. \quad (C6)$$

We find that FP2 exists when $0.08318 \leq \varepsilon$ because ε should be large enough to overcome the screening in $\beta_\alpha(\varepsilon > 2\tilde{\Gamma})$. It is stable only when $\varepsilon < 0.3103$. The anomalous dimensions are given by

$$z = 1.01 + 0.394\varepsilon, \quad \eta_\psi = -0.0427 + 3.46\varepsilon, \quad \eta_\Phi = 5\varepsilon,$$

$$\nu_m^{-1} = 1.08 - 1.99\varepsilon, \quad \nu_r^{-1} = 1.96 - 0.805\varepsilon. \quad (C7)$$

The other fixed points can be found in Table I. Most of them are either unphysical or unstable. The only stable fixed points are the fourth (FP1) and the last one (FP2), which are given in Eqs. (C3) and (C6), respectively. Stabilities of FP1 and FP2 can be checked with the linearized equations ($\Delta X \equiv X - X_*$):

$$\begin{pmatrix} \beta_{\Delta c} \\ \beta_{\Delta \alpha} \\ \beta_{\Delta \tilde{u}} \\ \beta_{\Delta \tilde{\Gamma}} \end{pmatrix} = \begin{pmatrix} c_* & 0 & 0 & 0 \\ 0 & \alpha_* & 0 & 0 \\ 0 & 0 & \tilde{u}_* & 0 \\ 0 & 0 & 0 & \tilde{\Gamma}_* \end{pmatrix} \begin{pmatrix} \alpha_* f'_1(c_*) & f_1(c_*) & 0 & -1 \\ -\alpha_* f'_2(c_*) & -f_2(c_*) & 0 & -2 \\ -\alpha_* f'_3(c_*) & -f_3(c_*) & -11 & 5 \\ -\alpha_* f'_4(c_*) & -f_4(c_*) & -4(6\sqrt{\pi}+1) & 3 \end{pmatrix} \begin{pmatrix} \Delta c \\ \Delta \alpha \\ \Delta \tilde{u} \\ \Delta \tilde{\Gamma} \end{pmatrix} + \begin{pmatrix} \frac{(\beta_c)_*}{c_*} \Delta c \\ \frac{(\beta_\alpha)_*}{\alpha_*} \Delta \alpha \\ \frac{(\beta_{\tilde{u}})_*}{\tilde{u}_*} \Delta \tilde{u} \\ \frac{(\beta_{\tilde{\Gamma}})_*}{\tilde{\Gamma}_*} \Delta \tilde{\Gamma} \end{pmatrix}. \quad (C8)$$

In Fig. 10, deviation from Eq. (C3) and that from Eq. (C5) go to zero in the low energy limit, so both FP1 and FP2 are infrared-stable.

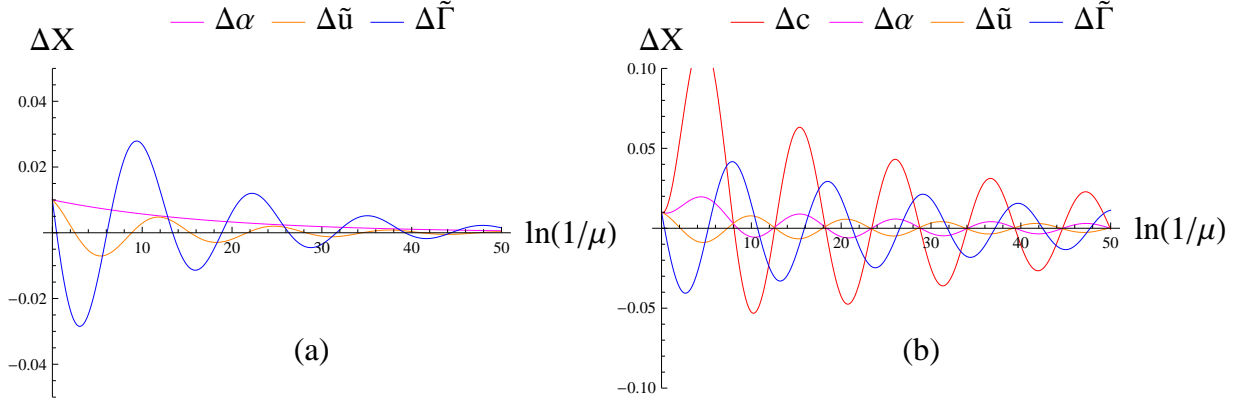


FIG. 10: Flowing of deviations of coupling constants (a) from Eq. (C3) and (b) from Eq. (C5)

Appendix D: Higher order corrections

We consider how the one-loop renormalized theory that we found is controlled even at higher orders. For simplicity, we write everything in a very schematic way.

1. Boson interaction and disorder scattering

We consider n -point correlation functions of the bosons, $\langle \Phi(q_1) \cdots \Phi(q_n) \rangle$. This correlation function is expanded in the loop order as

$$\sum_{V_u, \{p\}} (c^3 u_r)^{V_u} D^{I_b}(p_0 + q_0, c\mathbf{p} + c\mathbf{q}) = \sum_{V_u, \{p\}} \frac{(c^3 u_r)^{V_u}}{c^{3L}} D^{I_b}(p_0 + q_0, \mathbf{p} + c\mathbf{q}) = \sum_{V_u, \{p\}} u_r^{V_u} c^{\frac{3}{2}(E_b - 2)} D^{I_b}(p_0 + q_0, \mathbf{p} + c\mathbf{q}), \quad (\text{D1})$$

where \mathbf{p} (\mathbf{q}) are loop (external) momenta and V_u , I_b , and $E_b = n$ are the number of the vertices, the propagator, and the external fields. We rescaled $c\mathbf{p} \rightarrow \mathbf{p}$ in the second equality and used $L = I_b - V_u + 1$ and $V_u = \frac{1}{2}I_b + \frac{1}{4}E_b$ in the third equality. The boson Green's function ($E_b = 2$) is corrected with a factor of $u_r^{V_u} c^0$, while the boson scattering amplitude ($E_b = 4$) is corrected with $u_r^{V_u} c^3$. Here, we omit the vacuum energy ($E_b = 0$) since it's not observable. At FP1, we have $u_r \sim 4$ and $c \rightarrow 0$, so the Green's function is modified with a finite correction while the boson scattering amplitude vanishes at any order in the low-energy limit. At FP2, we have $u_r \sim 4$ and $c \sim 1$, so both the Green's function and the boson scattering amplitude are modified with a finite correction in every order. In the case of the disorder scattering, the result is the same.

2. Zeeman coupling term

We consider correlation functions of the fermions and the bosons:

$$\langle \psi(q_1) \bar{\psi}(q_2) \cdots \psi(q_{2n-1}) \bar{\psi}(q_{2n}) \Phi(q_{2n+1}) \cdots \Phi(q_{2n+m}) \rangle.$$

The correlation function is expanded in the loop order as

$$\sum_{V_\lambda, \{p\}} \lambda_r^{V_\lambda} G^{I_f}(p_0 + q_0, \mathbf{p} + \mathbf{q}) D^{I_b}(p_0 + q_0, c\mathbf{p} + c\mathbf{q}),$$

where \mathbf{p} (\mathbf{q}) are the loop (external) momenta and V_λ , $I_{f(b)}$, and $E_{f(b)} = 2n(m)$ are the number of the vertices, the fermion (boson) propagator, and the external fermion (boson) fields.

At FP2, we have $\lambda_r \sim \mathcal{O}(1)$, $c \sim 1$, so all correlation functions get a finite correction in every order. For FP2, this is the end of story. However, at FP1 there are singular factors coming from $c \rightarrow 0$. Note that unlike the interaction case,

there is no compensating c factor in the vertices. We estimate the enhancement factor coming from the low-frequency regime. In the limit of $c \rightarrow 0$ the boson propagator becomes $D(p_0) \sim |p_0|^{-(2-\eta_\Phi)/z}$. We take a cutoff as $p_0 = c|\mathbf{p}|$ and neglect p_0 in the fermion propagator. This is always possible because there are other terms like \mathbf{p} , m . Then, we find $\lambda_r^{V_\lambda} \left\{ \int^{c|\mathbf{p}|} d|p_0| |p_0|^{-(2-\eta_\Phi)/z} \right\}^{I_b} \sim \lambda_r^{V_\lambda} c^{(1-(2-\eta_\Phi)/z)I_b} = \lambda_r^{V_\lambda} c^{(1-(2-\eta_\Phi)/z)(V_\lambda-E_b)/2}$ where we used $V_\lambda = 2I_b + E_b$. Since λ_r and c decrease in the same rate as $\lambda_r \sim c \sim \exp(-\tilde{\Gamma}_* l)$, we find $c^{I(V_\lambda, E_b)}$, where

$$I(V_\lambda, E_b) = \left(\frac{3}{2} - \frac{2-\eta_\Phi}{2z} \right) V_\lambda - \left(\frac{1}{2} - \frac{2-\eta_\Phi}{2z} \right) E_b = \left(\frac{1}{2} + \mathcal{O}(\varepsilon) \right) V_\lambda + \left(\frac{1}{2} + \mathcal{O}(\varepsilon) \right) E_b. \quad (\text{D2})$$

The more vertices we add, the more rapidly the loop correction decreases because of decreasing λ_r and c . Thus, the loop expansion for the Zeeman coupling is controlled.

-
- [1] H. V. Lohneysen, *Electron-electron interactions and the metal-insulator transition in heavily doped silicon*, Ann. Phys. (Berlin) **523**, 599 (2011).
 - [2] V. Dobrosavljevic, *Introduction to metal-insulator transitions, in Conductor-Insulator Quantum Phase Transitions*, edited by V. Dobrosavljevic, N. Trivedi, and J. M. Valles Jr. (Oxford University Press, Oxford, 2012).
 - [3] T. Dietl, and H. Ohno, *Dilute ferromagnetic semiconductors: Physics and spintronic structures*, Rev. Mod. Phys. **86**, 187 (2014).
 - [4] Soo-Whan Kim, Jinsu Kim, Kyoung-Min Kim, Ki-Seok Kim, and Myung-Hwa Jung, *Weyl metals from magnetically doped semiconductors*, to be submitted.
 - [5] H.-J. Kim, K.-S. Kim, J.-F. Wang, M. Sasaki, N. Satoh, A. Ohnishi, M. Kitaura, M. Yang, and L. Li, *Dirac versus Weyl fermions in topological insulators: Adler-Bell-Jackiw anomaly in transport phenomena*, Phys. Rev. Lett. **111**, 246603 (2013); K.-S. Kim, H.-J. Kim, and M. Sasaki, *Boltzmann equation approach to anomalous transport in a Weyl metal*, Phys. Rev. B **89**, 195137 (2014); Ki-Seok Kim, Heon-Jung Kim, M. Sasaki, J.-F. Wang, and L. Li, *Anomalous transport phenomena in Weyl metal beyond the Drude model for Landau's Fermi liquids*, Sci. Technol. Adv. Mater. **15**, 064401 (2014).
 - [6] Dongwoo Shin, Yongwoo Lee, M. Sasaki, Yoon Hee Jeong, Franziska Weickert, Jon B. Betts, Heon-Jung Kim, Ki-Seok Kim, and Jeehoon Kim, *Violation of Ohm's law in a Weyl metal*, Nature Materials **16**, 1096 (2017), doi:10.1038/nmat4965.
 - [7] K.-M Kim, D.-W Shin, M. Sasaki, H.-J. Kim, J.-H. Kim, and K.-S. Kim, *Two-parameter scaling theory of the longitudinal magnetoconductivity in a Weyl metal phase: Chiral anomaly, weak disorder, and finite temperature*, Phys. Rev. B **94**, 085128, (2016).
 - [8] H.-J. Kim, K.-S. Kim, J.-F. Wang, V. A. Kulbachinskii, K. Ogawa, M. Sasaki, A. Ohnishi, M. Kitaura, Y.-Y. Wu, L. Li, I. Yamamoto, J. Azuma, M. Kamada, and V. Dobrosavljevic, *Topological phase transitions driven by magnetic phase transitions in $Fe_xBi_2Te_3$ ($0 \leq x \leq 0.1$) single crystals*, Phys. Rev. Lett. **110**, 136601 (2013).
 - [9] K.-M. Kim, Y.-S. Jho, and K.-S. Kim, *Dilute magnetic topological semiconductor*, Phys. Rev. B **91**, 115125 (2015).
 - [10] Iksu Jang, Jae-Ho Han, and Ki-Seok Kim, *Anomalous Hall effects beyond Berry magnetic fields in a Weyl metal phase*, Phys. Rev. B **95**, 054117 (2017); Yong-Soo Jho, Jae-Ho Han, and Ki-Seok Kim, *Topological Fermi-liquid theory for interacting Weyl metals with time reversal symmetry breaking*, Phys. Rev. B **95**, 205113 (2017); Iksu Jang and Ki-Seok Kim, *Chiral pair of Fermi arcs, anomaly cancellation, and spin or valley Hall effects in Weyl metals with broken inversion symmetry*, Phys. Rev. B **97**, 165201 (2018).
 - [11] M. Z. Hasan and C. L. Kane, *Colloquium: Topological insulators*, Rev. Mod. Phys. **82**, 3045 (2010); X.-L. Qi, and S.-C. Zhang, *Topological insulators and superconductors*, Rev. Mod. Phys. **83**, 1057 (2011).
 - [12] M. A. Ruderman and C. Kittel, *Indirect exchange coupling of nuclear magnetic moments by conduction electrons*, Phys. Rev. **96**, 99 (1954); T. A. Kasuya, *Theory of metallic ferro- and antiferromagnetism on Zener's model*, Prog. Theor. Phys. **16**, 45 (1956); K. Yosida, *Magnetic properties of Cu-Mn alloys*, Phys. Rev. **106**, 893 (1957).
 - [13] Boyanovsky, Daniel and Cardy, John L., *Critical behavior of m-component magnets with correlated impurities*, Phys. Rev. B **26**, 154 (1982).
 - [14] J. Zinn-Justin, *Quantum Field Theory and Critical Phenomena*, Clarendon Press 1989 (Oxford 4th ed. 2002).
 - [15] H. B. Nielsen, and M. Ninomiya, *The Adler-Bell-Jackiw anomaly and Weyl fermions in a crystal*, Phys. Lett. B **130**, 389 (1983).
 - [16] F. D. M. Haldane, *Berry curvature on the Fermi surface: Anomalous Hall effect as a topological Fermi-liquid property*, Phys. Rev. Lett. **93**, 206602 (2004).
 - [17] S. Murakami, *Phase transition between the quantum spin Hall and insulator phases in 3D: Emergence of a topological gapless phase*, New J. Phys. **9**, 356 (2007).
 - [18] A. A. Burkov and L. Balents, *Weyl semimetal in a topological insulator multilayer*, Phys. Rev. Lett. **107**, 127205 (2011).
 - [19] Bitan Roy, Vladimir Juricic, and Igor F. Herbut, *Emergent Lorentz symmetry near fermionic quantum critical points in two and three dimensions*, J. High Energ. Phys. **2016**: 18 (2016).